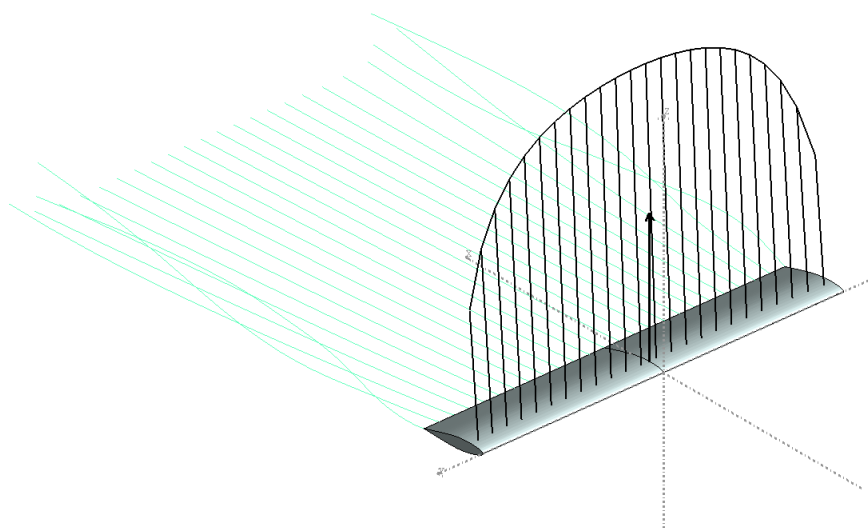


Manual for Low Speed Windtunnel Test AE2130-II

2D and 3D aerodynamic characteristics of a straight, low aspect ratio wing



Version 1.6
November 2024

L.L.M. Veldhuis
updated and revised by M. Kotsonis & M. Li

Summary

This manual contains a short description of the AE2130-II windtunnel test as well as some background material to work out the assignment. Additional information on airfoils and wings may be found in the book of J.D. Anderson, “*Fundamental of Aerodynamics*” ([1]) and some other references given herein. The goal of the practical is to get a better insight in the lecture material that is treated in the AE 2130 course, Aerodynamics I. Moreover the effects of viscosity and the resulting development of the boundary layer play an important role in this windtunnel test.

To learn more about the capabilities and limitations of several numerical models for the analysis of 2D and 3D flow, a comparison is made between experimental and numerical data. The methods chosen for the numerical approach are mainly based on the theory covered so far in the courses on aerodynamics. For this, existing software will be used that is available for students through the Internet. At a later stage students are encouraged to determine carefully the possibilities but certainly also the limitations that these programs have.

Suggestions for preparation of the lab report and questions to be answered are treated in this manual as well. Additional resources are available through the appropriate pages on Brightspace.

Nomenclature

α	angle of attack
α_0	zero lift angle of attack
α_i	induced angle of attack
$\delta_1, \delta_2, \delta_3$	airfoil related angles in thin wing theory
Γ	circulation strength
γ	local vorticity strength
ϕ	velocity potential
ρ	air density
θ	local airfoil contour angle
A	wing aspect ratio
A_i	fourier coefficients
b	wing span
c	airfoil chord
C_d	two dimensional drag coefficient
C_L	three dimensional lift coefficient
C_l	two dimensional lift coefficient
C_m	pitching moment coefficient
C_n	normal force coefficient
C_p	pressure coefficient
C_{D_i}	induced drag coefficient
C_{D_p}	wing profile drag coefficient
$C_{m,n}$	influence coefficients in panel analysis
C_{p_t}	total pressure coefficient
D	drag force
D_i	induced drag force
l	local lift per meter
M	pitching moment
N	normal force
p	pressure
p_t	total pressure

q_∞	undisturbed dynamic pressure
r	radial coordinate
Re	Reynolds number
S	wing reference area
s	coordinate along the contour of the airfoil
u, v, w	velocity components in x , y , and z direction
V_∞	undisturbed wind speed
x, y, z	airfoil coordinate system

Contents

1	Introduction	7
2	Theoretical background	8
2.1	Introduction	8
2.2	Force and moment from pressure distributions	8
2.3	2D Airfoil characteristics	10
2.4	Flow phenomena	12
2.4.1	Hysteresis	12
2.5	3D wing characteristics	14
2.5.1	The finite wing	14
2.5.2	Lift coefficient	16
2.5.3	Induced drag	17
2.5.4	Comparison with elliptical wing	18
3	Experimental setup	21
3.1	Windtunnel	21
3.2	Model	22
3.3	Data files	22
4	Numerical methods	24
4.1	Numerical methods 2D	24
4.1.1	Aerodynamic characteristics of airfoils	24
4.1.2	Thin airfoil theory	25
4.1.3	Planar (symmetrical) airfoil	26
4.1.4	Symmetrical airfoil properties	26
4.1.5	Inviscid/Viscous 2D panel code (XFOIL or XFLR5)	28
4.2	Simple Numerical methods in 3D	32
4.2.1	Lifting Line Theory	32
4.2.2	Non-linear lifting Line Theory	33
4.2.3	Vortex Lattice Code	33
5	Post-processing and reporting	36
5.1	Introduction	36
5.2	Work-load reporting	36
5.3	Deadlines	36
5.4	Tasks	36
5.5	Typical contents of the lab report and rubrics	37

<i>CONTENTS</i>	6
Appendix A Overview of activities during Windtunnel test AE2130-II	39
Appendix B Location	41
Appendix C About graphs	43

Chapter 1

Introduction

Windtunnels have played an important part in the development of aircraft over been the last 100 years. Already in 1901 the Wright brothers utilized a small windtunnel to find the characteristics of airfoils and wings (fig. 1.1). In modern times the application of windtunnels besides modern computational techniques is based on the fact that even fast computers running the most sophisticated software are not able to predict the flow behaviour in all details or to an acceptable level of accuracy in some cases. In this respect experimental windtunnel research and numerical research, often denoted as "Computational Fluid Dynamics" (CFD) are complimentary. Nowadays, very often windtunnels are used to validate the computational codes that are developed (ref. [2]).

In this practical we will do just that: see how well models for the calculation of airfoils and wings predict the real flow that is found in a windtunnel test. For this purpose experiments will be performed on a straight wing model which can be installed as a "2-dimensional" wing (which shows the airfoil characteristics) and a "3-dimensional" wing which shows the effects of rolled up vortex sheets and wing tips. The experimental part consists of balance and surface pressure measurements which will all be performed by students. To determine the laminar / turbulent state of the boundary layer an infrared camera will be used. Additionally, tufts will be used for flow visualization.

During and after the experimental work, numerical predictions need to be produced by the provided tools (Brightspace) and included in the final report. For the comparison of 2D airfoil data of experiments and CFD the XFOIL code is available. This code is quite accurate and it is used by many airfoil designers. The computational codes that are used to determine the wing characteristics will be limited to two quite simplified models: the well known *lifting line theory* and a *vortex lattice method*. As will be shown later, the effects of viscosity (which leads to the development of a boundary layer) will play a crucial role in the flow behavior and the associated airfoil and wing characteristics.

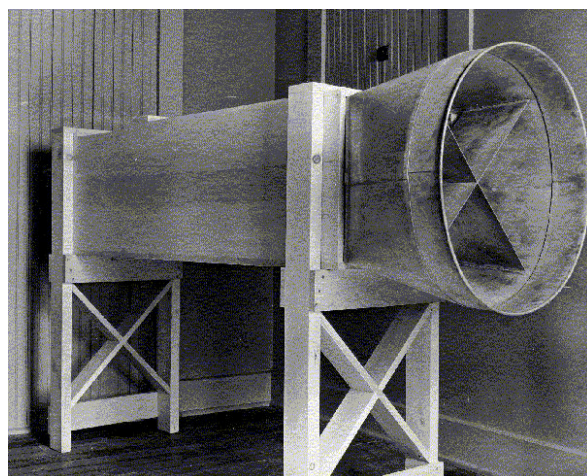


Figure 1.1: Replica of the windtunnel used by the Wright brothers for fundamental research they did in aerodynamics in the winter of 1901-1902.

Chapter 2

Theoretical background

2.1 Introduction

In this chapter some of the concepts, as presented in ref. [1] are repeated to get a decent starting point for the execution of the experiments and the calculations. Various other works (refs. [3, 1, 5]) provide useful information as well. Moreover information about the practical is provided though the University Brightspace pages.

2.2 Force and moment from pressure distributions

From the pressure distribution over the airfoil and in the wake the characteristic forces and moments can be obtained. The various geometrical and aerodynamic parameters of a 2-dimensional airfoil are presented in fig. 2.1.

The normal force coefficient follows directly from the (static) pressure distribution over the upper and lower side of the airfoil. This can be seen as follows.

The contribution of an element with length ds at which pressure p acts is:

$$dN = -pds \cos \theta$$

The normal force than follows from integration over the surface:

$$N = - \oint_s p \cos \theta ds$$

With $ds \cos \theta = dx$ we find:

$$N = - \int_0^c p_u dx + \int_0^c p_l dx$$

where the indices u and l refer to the upper and lower side of the airfoil respectively. The dimensionless normal force coefficient now becomes:

$$C_n = \frac{N}{\frac{1}{2} \rho U_\infty^2 c} = - \int_0^1 \frac{p_u - p_l}{\frac{1}{2} \rho U_\infty^2} d \frac{x}{c}$$

This can be written in the form an integral over the pressure coefficient which is defined as:

$$C_p = \frac{p - p_\infty}{\frac{1}{2} \rho V_\infty^2} = \frac{p - p_\infty}{q_\infty}$$

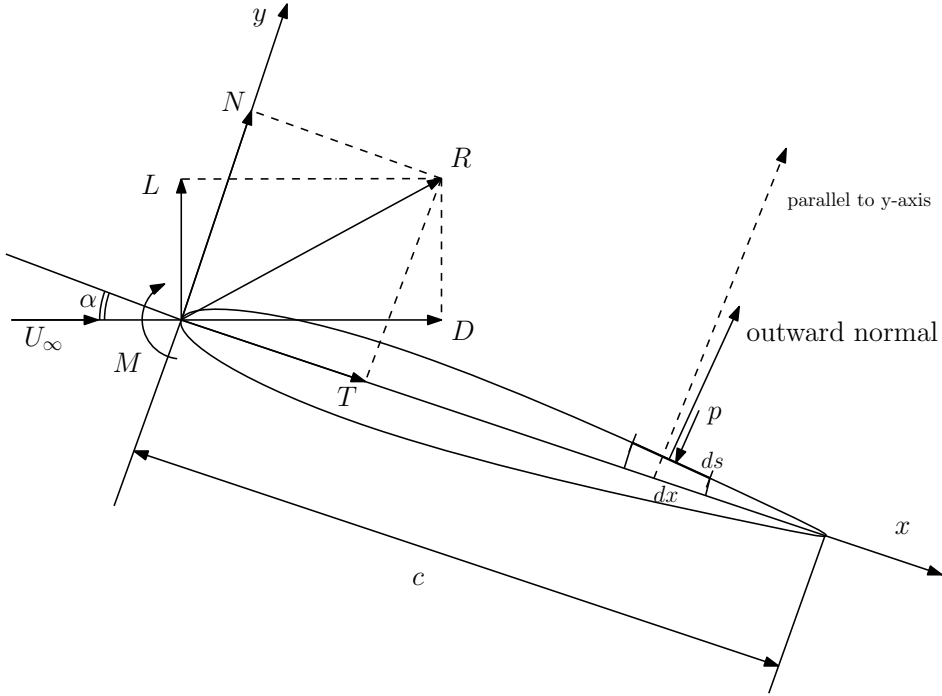


Figure 2.1: Aerodynamic and geometrical parameters of a 2-dimensional airfoil.

Hence

$$C_n = \int_0^1 (C_{p_l} - C_{p_u}) d\frac{x}{c} \quad (2.1)$$

Note that in eq. 2.1 the minus sign has been incorporated in the integral (C_{p_u} and C_{p_l} have switched places).

The pitching moment coefficient of the airfoil can be obtained in an analogue way:

$$C_m = \frac{M}{q_\infty c^2} = \int_0^c \frac{(p_u - p_l) x}{q_\infty c^2} dx$$

$$C_m = \int_0^1 (C_{p_u} - C_{p_l}) \frac{x}{c} d\frac{x}{c}$$

The moment with respect to the quarter-chord point follows from

$$M_{0.25c} = M_{le} + 0.25c \times N$$

or

$$C_{m_{0.25c}} = C_{m_{le}} + 0.25 \times C_n$$

The drag coefficient of the airfoil follows from application of the momentum equation on a control volume (see section 2.6 of ref. [1]). Using the notations of fig. 2.2 we may find the drag force from:

$$D = \rho \int_{wake} u_2 (U_\infty - u_2) dy_2 \quad (2.2)$$

Recall that this result is obtained only in the case that the pressure over the control volume is taken constant (being p_∞). In this case eq. 2.2 can be written in the form of coefficients:

$$C_d = \frac{1}{q_\infty} \int \rho u_2 (U_\infty - u_2) d\frac{y_2}{c} = \frac{2}{c} \int \frac{u_2}{U_\infty} \left(1 - \frac{u_2}{U_\infty} \right) dy_2 = 2 \frac{\theta}{c} \quad (2.3)$$

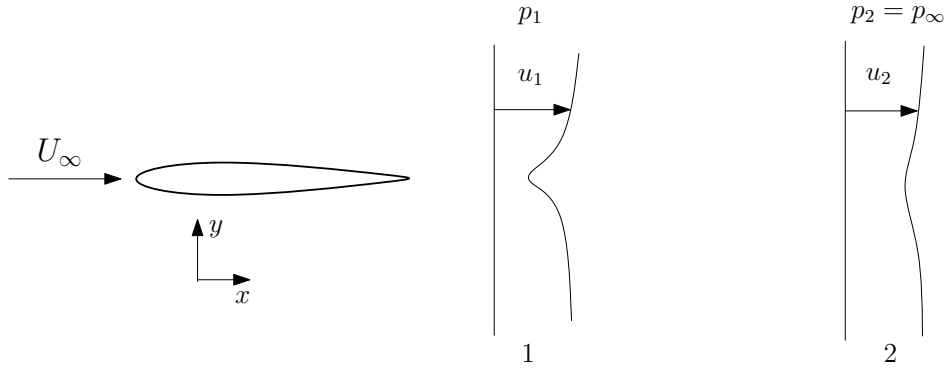


Figure 2.2: Drag analysis of an 2-dimensional airfoil.

The variable θ is called the momentum thickness, $\theta = \int \frac{u}{U_\infty} \left(1 - \frac{u}{U_\infty}\right) dy$ (for more information see ref. [1], section 17.2). Equation 2.3 can also be expressed in pressure coefficients

$$C_d = 2 \int \sqrt{\frac{p_{t2} - p_\infty}{q_\infty}} \left[1 - \sqrt{\frac{p_{t2} - p_\infty}{q_\infty}} \right] d\frac{y_2}{c}$$

or

$$C_d = 2 \int \sqrt{C_{p_t}} \left(1 - \sqrt{C_{p_t}} \right) d\frac{y_2}{c},$$

where $C_{p_t} \equiv (p_{t2} - p_\infty)/q_\infty$ is the total pressure coefficient (note that along a streamline the total pressure remains constant, $p_{t1} = p_{t2} = p_t$). However, the condition of constant pressure over the control volume in general does not hold; the wake is installed rather close to the model (location 1 in fig. 2.2) due to limited length of the test section. Hence we need to take into account a static pressure at the outflow boundary (1) which is not equal to the undisturbed value, $p_1 \neq p_\infty$. Equation 2.2 then becomes

$$D = \rho \int_{wake} u_1 (U_\infty - u_1) dy_1 + \int_{wake} (p_\infty - p_1) dy_1. \quad (2.4)$$

The lift force that acts on the airfoils now simply follows from the relation between the lift, drag, normal force and tangential force coefficients

$$\begin{aligned} C_l &= C_n \cos \alpha - C_t \sin \alpha \\ C_d &= C_t \cos \alpha + C_n \sin \alpha \end{aligned}$$

The quantities that are measured directly are the normal force coefficient, C_n and the drag coefficient, C_d . Hence the lift coefficient follows from

$$C_l = C_n \left(\cos \alpha + \frac{(\sin \alpha)^2}{\cos \alpha} \right) - C_d \tan \alpha \quad (2.5)$$

2.3 2D Airfoil characteristics

To enable useful comparisons between various airfoils typical characteristics plots. Airfoil and aircraft "polars" have been used for a long time in aeronautics. The correct German term is "Lilienthal'sches Polardiagramm", indicating that this method of graphing results of airfoil tests as has been used first by the famous Otto Lilienthal. He plotted the lift and drag forces of his experimental results as lift versus drag, as we still use it today (using coefficients instead of the actual forces). Additional graphs have been developed to plot relations between other coefficients in a similar way.

Typical polar plots that you will determine are:

- The "lift polar" (fig. 2.3a). This graph shows the lift coefficient C_l , plotted versus the angle of attack α . Typical features are the lift curve slope, a_0 and the value of the maximum lift coefficient, $C_{l_{max}}$. Moreover it may be used to get information about the stall behavior (in case of computational results presuming that the analysis code is able to make a realistic prediction of the viscous effects at large angle of attack where flow separation occurs)

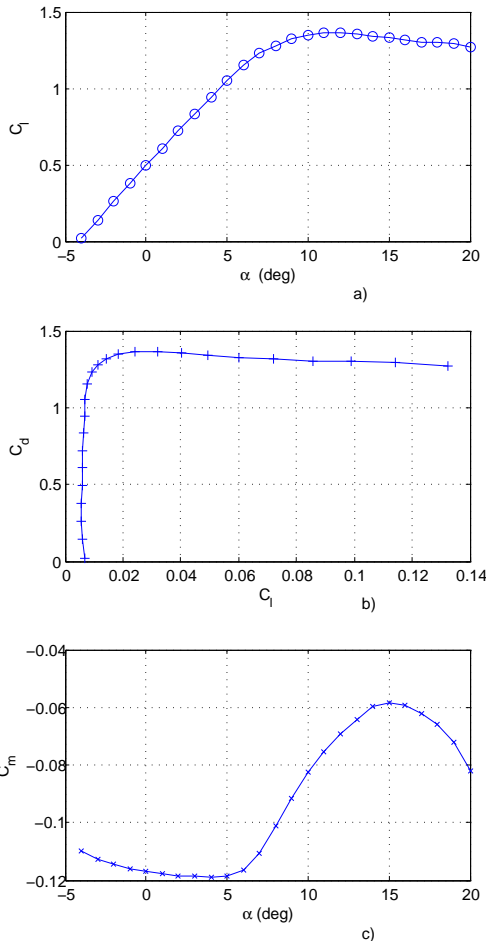


Figure 2.3: Example of calculated lift (a), drag (b) and pitching moment (c) polars. NACA63619 airfoil at $Re = 2.0 \times 10^6$.

- The “drag” polar (fig. 2.3b). This graph specifies the drag coefficient C_d for a given lift coefficient C_l . This is often the most important part of the results and can be used to find the best climb or sink rate as well as the optimum glide angle ideally possible with this airfoil from the C_l/C_d ratio. For some airfoils the so called “low drag bucket” is visible.
- The pitching moment polar (fig. 2.3c). This plot is similar to the lift polar, but shows the moment coefficient C_m of the airfoil section instead of the lift coefficient versus the angle of attack α .

There are various reference works that provide airfoil data, the most famous of which is the book titled “Theory of Wing Sections” of Abbott and van Doenhoff (ref. [3]) containing polars of NACA airfoils. Ref. [4] provides data of more modern airfoils.

From these polars the behavior of the airfoils, as they are locally found at different cross sections of the wing, can be determined and their contribution to the integral wing characteristics can be estimated. For example: if the 2D airfoil reaches its highest lift coefficient, $C_{l_{max}}$ at a certain angle of attack $\alpha_{C_{l_{max}}}$ the wing will locally reach $C_{l_{max}}$ at the same effective angle of attack $\alpha_{eff} = \alpha_{C_{l_{max}}}$. This means that the effect of the downwash produced by the trailing vortex system is accurately taken into account.

The most important features/characteristics that may be found (depending on the airfoil shape) for the airfoil are presented in fig. 2.4. During the lab, additional information will be provided regarding these very important phenomena. The student is encouraged to study further material in open literature to familiarize himself¹ with given concepts.

¹Throughout this manual the male form is used. In all relevant cases the text applies to both male and female students.

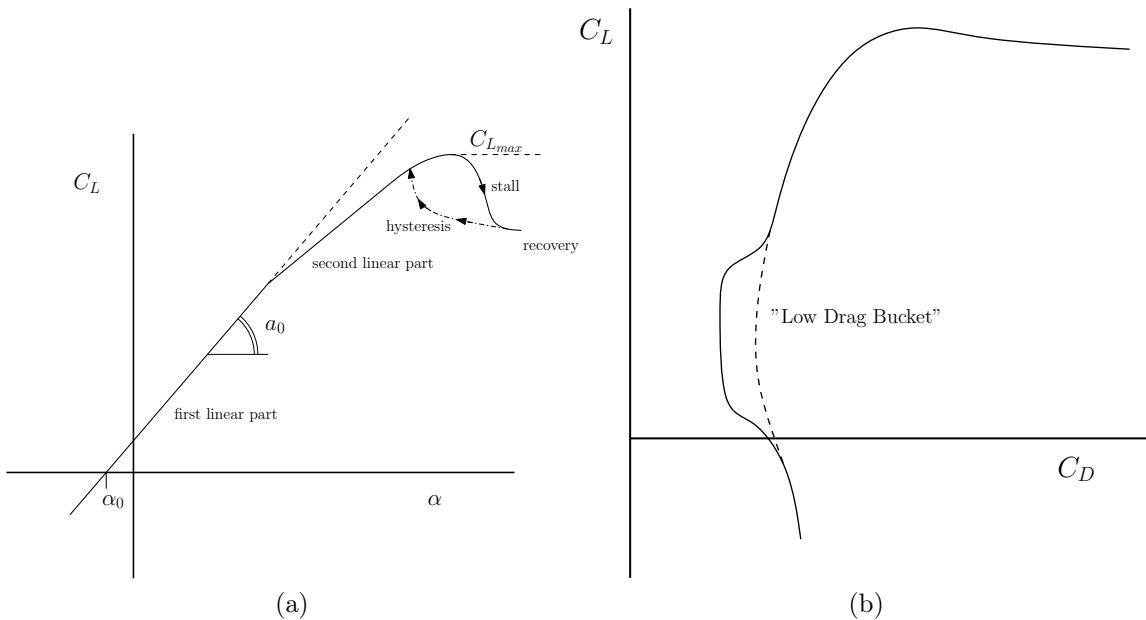


Figure 2.4: Typical features of the lift (a) and the drag (b) polar that may be found during the windtunnel tests.

2.4 Flow phenomena

On the airfoil a number of complex flow phenomena may occur like:

- Laminar flow
- Laminar separation bubble. This is a sequence of:
 - laminar separation
 - transition
 - reattachment
- Turbulent flow
- Turbulent separation

These presence of these characteristic flow phenomena can be determined with various techniques like: surface pressure measurements, wake rake (like boundary probes or hot wires), tufts and an infrared camera. In fig. 2.5 some of these phenomena are sketched as they occur over an NACA 64015 airfoil.

At relatively low Reynolds numbers the so-called Laminar Separation Bubble (fig. 2.6) greatly influences the local pressure distribution. At large angles of attack a separation bubble at the airfoil nose may burst open. The flow is then completely separated from the leading edge on. This leading edge stall is quite abrupt and dangerous as it is accompanied by a considerable loss in lift.

A well designed airfoil exhibits so called trailing edge stall. In that case the turbulent boundary layer starts separating from the trailing edge and with increasing angle of attack the separation point moves forward. Stall is then a continuous process. Since the viscous effects play a major role in the final aerodynamic characteristics of the wing it is very important to determine whether or not they are found on this model and to what extend they influence the pressure distribution. Sketches of phenomena encountered during the lab may help you in the post processing of the data and the discussion of the results.

2.4.1 Hysteresis

At large angles of attack the flow over the upper side of the wing will separate due to the strong adverse pressure gradients². This leads to significant loss in lift and a considerable increase drag.

²In later lectures on viscous flows the relation between flow separation and the pressure gradient will be elucidated through the application of the so called ‘‘boundary layer equations’’.

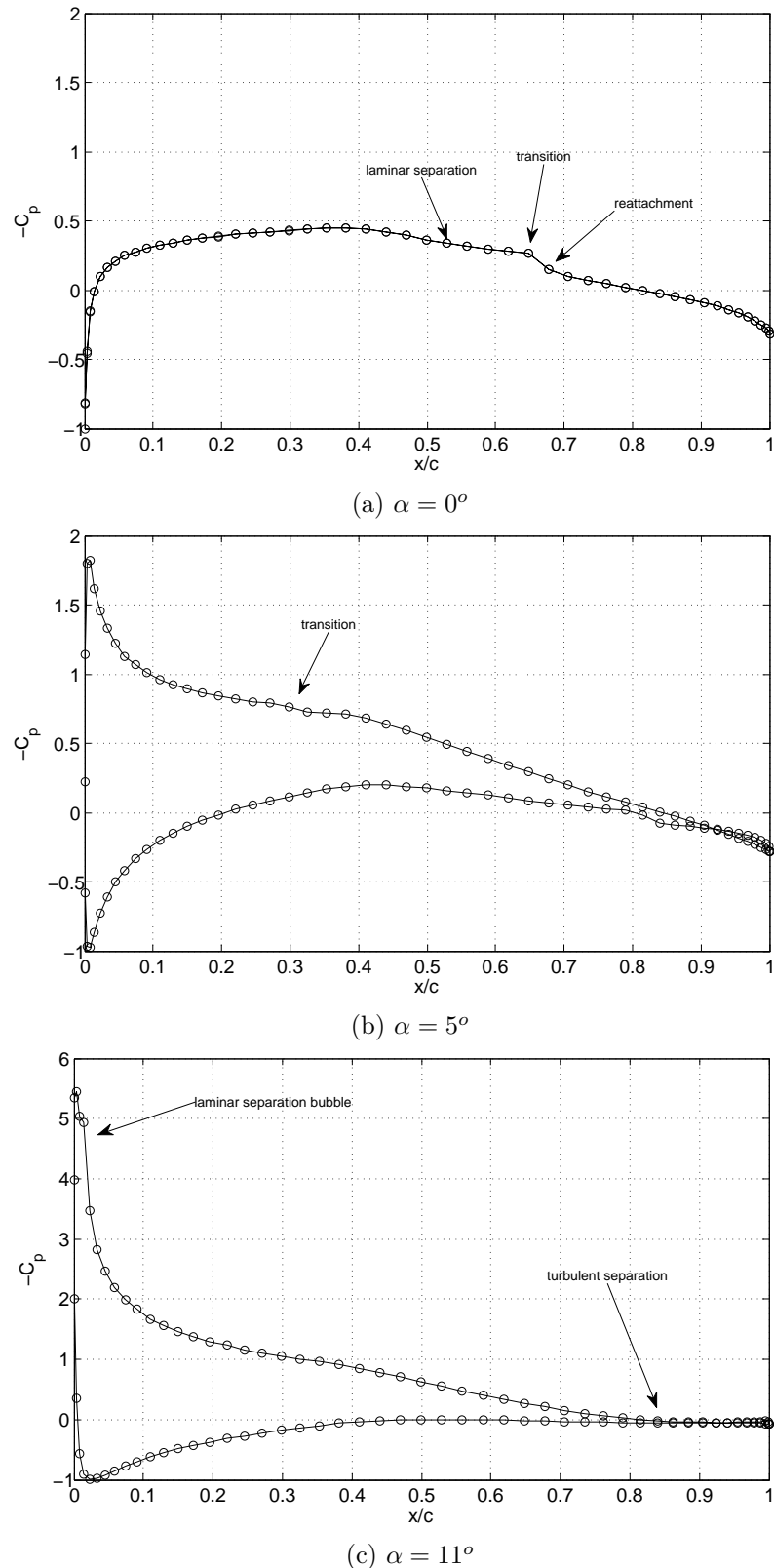


Figure 2.5: Typical flow phenomena occurring over a low speed airfoil and the associated pressure distribution. NACA 64015 airfoil at $Re = 8.3 \times 10^5$.

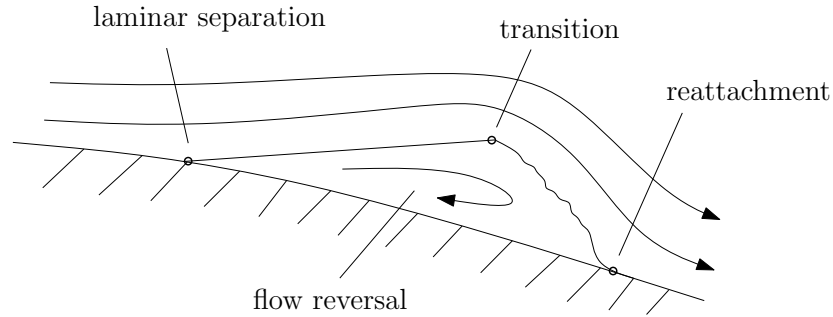


Figure 2.6: Flow pattern around a laminar separation bubble.

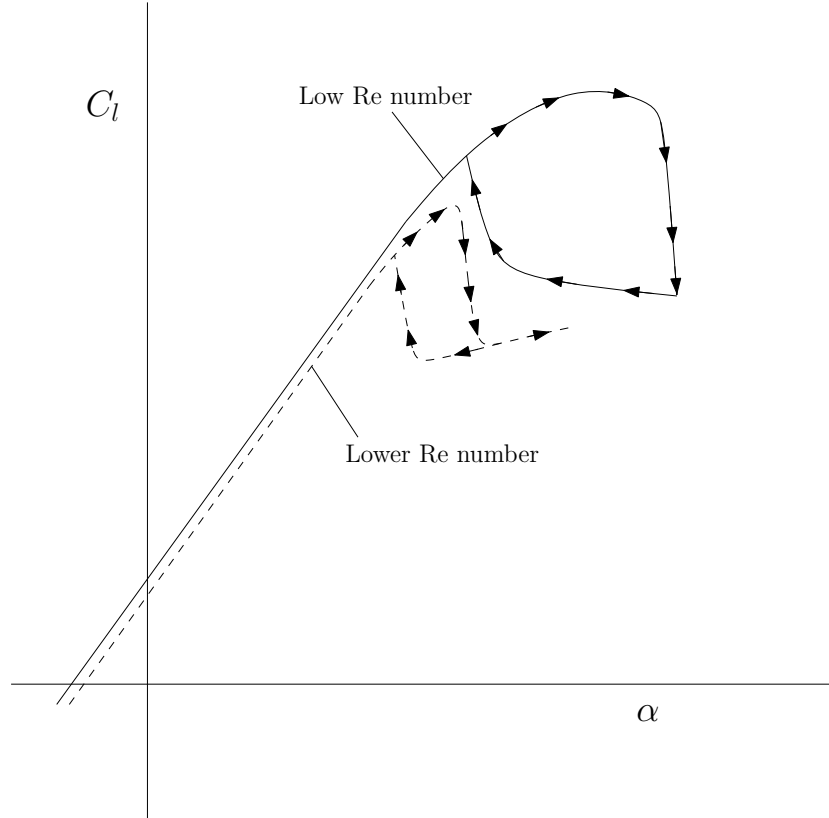


Figure 2.7: Typical hysteresis loops of an airfoil at low Reynolds numbers.

Since the pressure distribution in the separated flow case has altered in many cases it requires a large angle of attack decrease before the flow reattaches again. This phenomenon is known as aerodynamic hysteresis (fig. 2.7). The length of the hysteresis loop is a function of the Reynolds number. In some cases large loops lead to a dangerous flight condition for the aircraft. During the windtunnel test this important phenomenon, that can hardly be predicted by computer programs, will be investigated in detail.

2.5 3D wing characteristics

2.5.1 The finite wing

Once the table is removed from underneath the model and the wing tip is installed the flow becomes 3-dimensional as is typically found on airplane wings. Especially the fact that the flow now can move over the tip results in the generation of a tip vortex (fig. 2.8). You should realize that this tip vortex is not produced instantly but rather develops in chordwise direction (fig. 2.9). The vortex sheets that was initially flat now rolls up to produce a completely rolled vortex at some distance behind the wing (fig. 2.10).

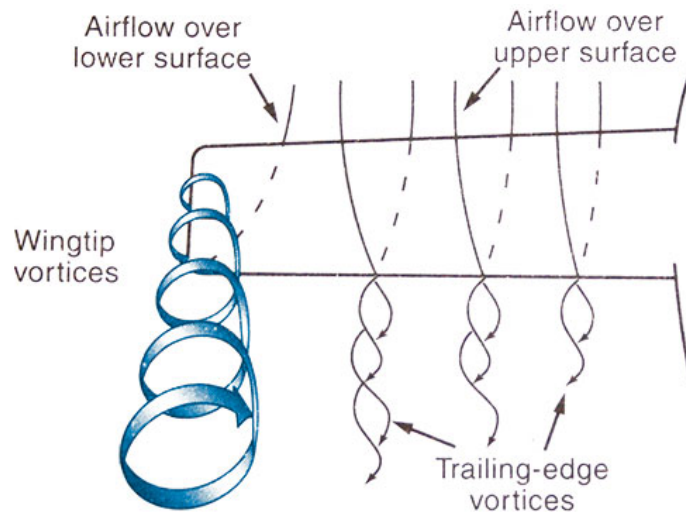


Figure 2.8: The generation of a tip vortex on a 3-dimensional wing.

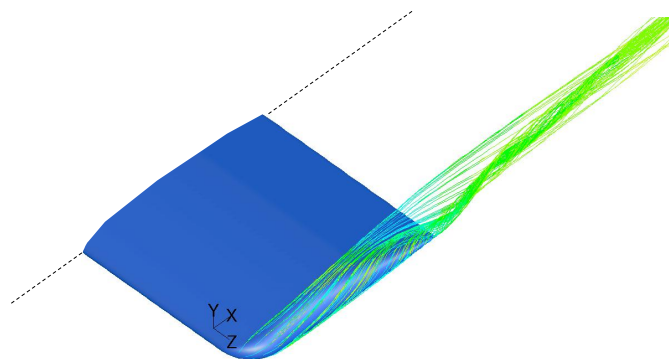


Figure 2.9: Development of a wing tip vortex in chordwise direction. CFD calculation on the practicum model.

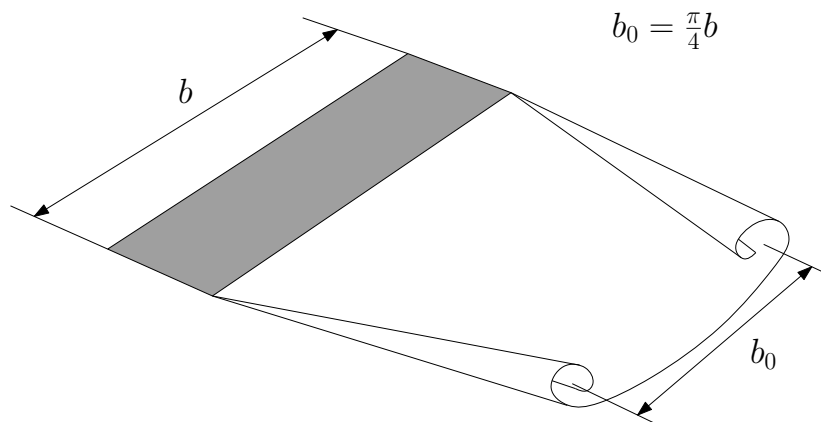


Figure 2.10: Vortex sheet roll up.

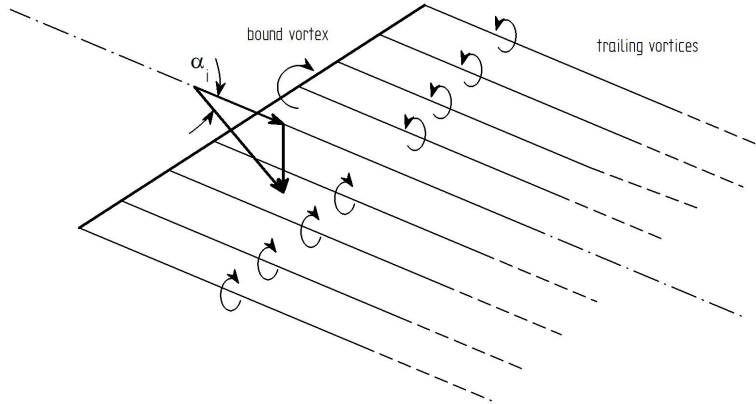


Figure 2.11: Local induced angle of attack due to bound and trailing vortex system.

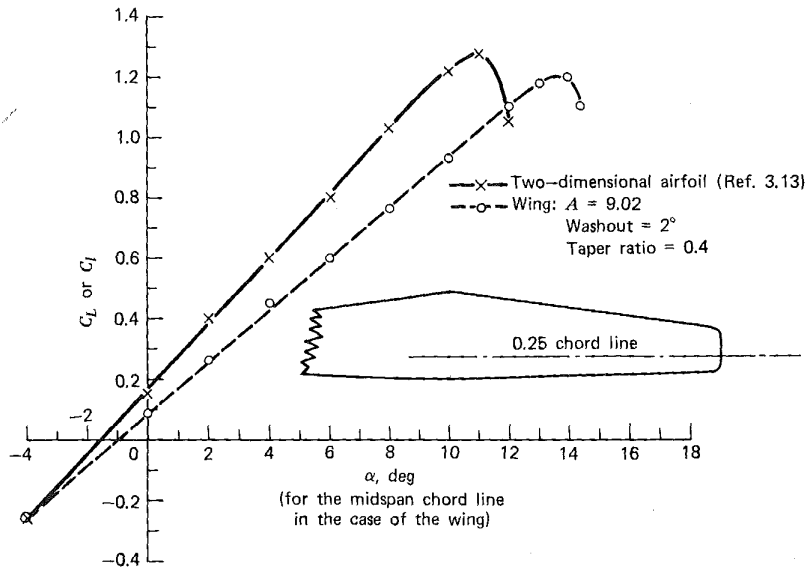


Figure 2.12: Comparison of a NACA 65-210 airfoil lift polar with of a wing using the same airfoil.

The presence of the trailing vortex system leads to an additional induced angle of attack that has a different value for all spanwise wing positions (fig. 2.11). In turn this induced angle of attack leads to the well known shape of the lift distribution over a wing.

2.5.2 Lift coefficient

As a result of the 3-dimensionality of the flow the lift, drag and lifting moment coefficients change considerably. As has been shown in ref. [6] the 3-dimensional lift coefficient of the wing is a function of the 2-dimensional coefficient and the wing aspect ratio. This can be expressed in a 3D lift curve slope for a wing that has an elliptical lift distribution (which is not necessarily the case for our windtunnel model!):

$$C_{L\alpha} = C_{l\alpha} \left(\frac{1}{1 + \frac{C_L}{\pi A}} \right) \quad (2.6)$$

Apparently the effect of the limited aspect ratio is to decrease the slope. A typical example is provided in fig. 2.12.

Eq. 2.6 is an important result that follows from the lifting line theory (see the discussion in section 4.2.1 and ref. [1]). A wing with a low aspect ratio will require a higher angle of attack than a wing with a greater aspect ratio in order to produce the same value of C_L . This is why for example the



Figure 2.13: Concorde in landing phase. Due to the low aspect ratio wing the angle of attack to maintain enough lift is very large. The nose of the cockpit needs to be tilted downward to allow visual contact with the runway.

Concorde (low aspect ratio wing) needs a movable nose during landing as the angle of attack attack is very large in this case (fig. 2.13). It allows the pilot to keep an eye on the runway.

As the aspect ratio decreases the lifting line theory, on which eq. 2.6 is based, becomes progressively less accurate. For example, for an aspect ratio of 4.0, eq. 2.6 produces a value 11% higher than that predicted by more accurate methods. Ref. [6] produces a more accurate estimate known as the *Helmbold equation*

$$C_{L_\alpha} = C_{l_\alpha} \frac{A}{\left(\frac{C_{l_\alpha}}{\pi} + \sqrt{\left(\frac{C_{l_\alpha}}{\pi} \right)^2 + A^2} \right)} \quad (2.7)$$

In case we replace C_{l_α} with 2π (thin wing theory) eq. 2.7 becomes

$$C_{L_\alpha} = C_{l_\alpha} \frac{A}{(2 + \sqrt{4 + A^2})} \quad (2.8)$$

With the know value for A and an assumed value for C_{l_α} (from the 2D airfoil characteristics) the value of the lift gradient may be determined using eq. 2.8. This value can directly be compared with experimental value that is obtained from the lift polar.

2.5.3 Induced drag

As described in ref. [1] the so called (lift) induced drag exists only for 3D wings. Its existence can be explained either through the tilting of the local lift vector (fig. 2.14) or as a result of the production of cross flow energy. In the latter case the drag follows (eq. 2.9) from the so called Trefftz plane analysis which will be treated in later lectures.

$$D_i = \frac{\rho}{2} \iint_{Trefftz\ plane} (v^2 + w^2) dA \quad (2.9)$$

As explained in Chapter 5 of ref. [1] the induced drag of a wing carrying an elliptical load distribution can be expressed simply as:

$$C_{D_i} = \frac{C_L^2}{\pi A}$$

where A denotes the aspect ratio given by $A = b^2/S$. It should not be a surprise that the wing that is tested in this windtunnel test exhibit a lift distribution that is not quite elliptical (as most wings do

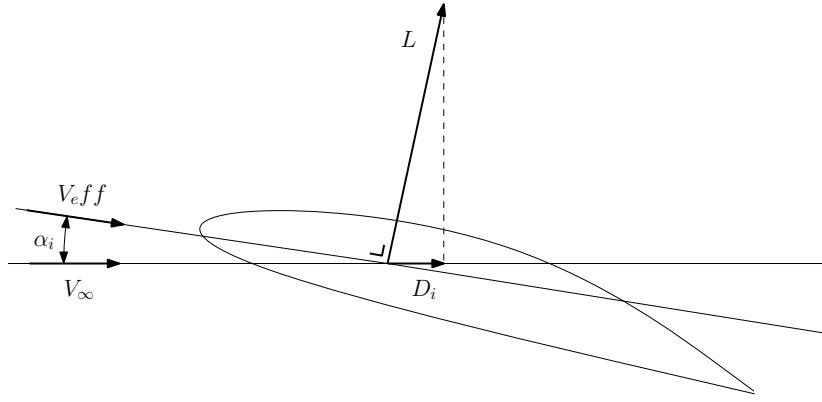


Figure 2.14: Induced drag explained as a resulting of a tilted lift vector. The induced angle of attack, α_i is the result of the trailing vortex system behind a 3-dimensional wing.

by the way). The increase in the induced drag that is the result of this is expressed in the well known **span efficiency factor**, e which (for planar wings³) is smaller than 1. The induced drag then becomes

$$C_{D_i} = \frac{C_L^2}{\pi A e}$$

As during the windtunnel test the total drag coefficient of the 3D wing

$$C_D = C_{D_p} + C_{D_i}$$

is measured with an external balance it will be impossible to separate the induced drag coefficient, from the profile drag coefficient, C_{D_p} . A Trefftz plane analysis method, employing eq. 2.9 (or even better a so-called "Quantitative Wake Analysis method", ref. [8]), would be necessary to obtain the induced drag separately.

For additional considerations regarding the induced drag the reader is referred to refs.[1] and [5].

2.5.4 Comparison with elliptical wing

To check whether that the properties of wings of arbitrary planform (as our WT model) can be approximated by those of the elliptical wing, some of the results derived for the elliptical wing theory are now compared with some experimental data that can be found in open literature.

Let us consider an untwisted wing having identical symmetrical airfoil sections along the span. With the assumption of an elliptical lift distribution, all the angles of attack are invariant along the wing span (argue why!) and the zero lift angle of attack, α_{L0} is zero. In this case the geometrical angle of attack becomes (see fig. 2.15)

$$\alpha = \alpha_0 + \frac{C_L}{\pi A} \quad (2.10)$$

To get insight about the validity of elliptical wing loading 7 rectangular wings of aspect ratios varying from 1 to 7 were tested in a windtunnel. as reported by Prandtl (1921 !) . In fig. 2.16 the measured wing-lift coefficient C_L is plotted versus the geometrical angle of attack α for each of those wings.

According to the fact that $\alpha_0 = \alpha_a - \alpha_i$, for a given C_L , wings of different aspect ratios will have the same effective angle of attack α_0 . Under such a condition and by referring to a $A = 5$ wing whose geometrical angle of attack is α' , equation (2.10) yields

$$\alpha' = \alpha + \frac{C_L}{\pi} \left(\frac{1}{5} - \frac{1}{A} \right)$$

Based on this conversion formula, the experimental data points for different A values shown in fig. 2.16 a collapse onto a single curve when C_L is plotted versus α' in fig. 2.16b. The phenomenon may

³In case of non-planar wings for example those with a large dihedral or wings equipped with a winglet, the span efficiency factor actually may become larger than 1 even if the load distribution is non-elliptical.

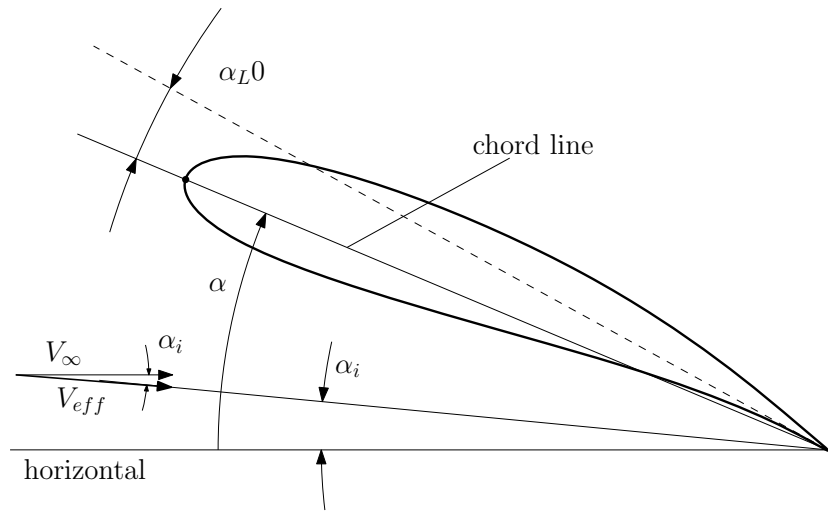
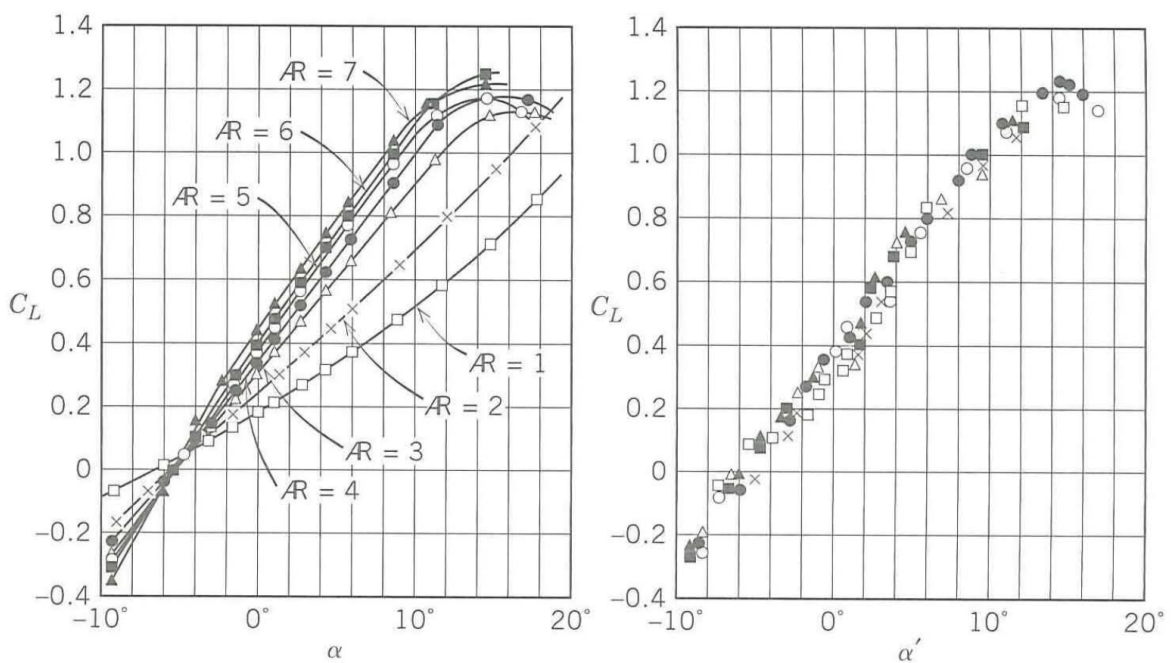


Figure 2.15: Definition of the angles of attack for an airfoil.

Figure 2.16: Experimental test of rectangular wings of $A = 1 - 7$ (Prandtl, 1921). In these figures the symbol AR denotes the aspect ratio A .

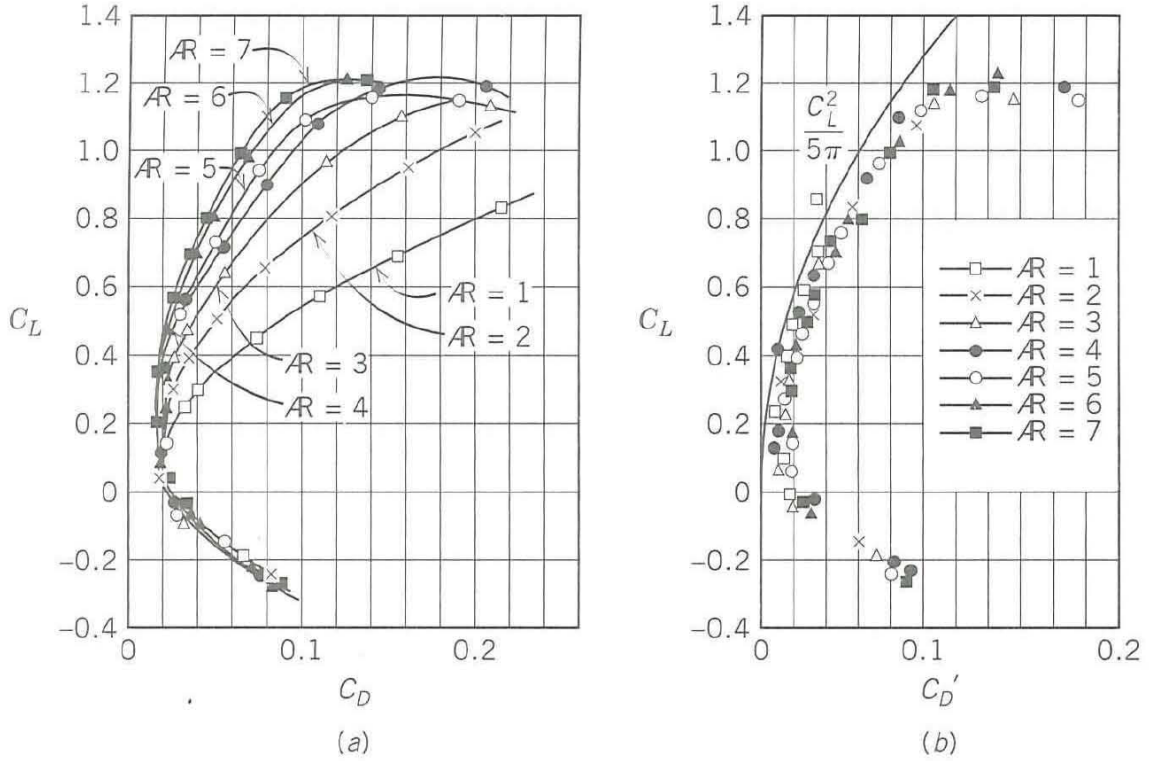


Figure 2.17: Experimental test of calculated C'_D for rectangular wings of $1 \leq A \leq 7$ after Prandtl (1921).

be interpreted as follows: for the same lift coefficient, the wing of aspect ratio A flying at an angle of attack α is equivalent to an $A = 5$ wing at an angle of attack α' .

The plots presented in fig. 2.17 are termed "polar plots" for the wing . In fig. 2.17a, C_L is plotted against C_D , defined by

$$C_D = C_{D_0} + C_{D_i}$$

where C_{D_0} is the profile drag coefficient caused by viscosity consisting of skin friction and pressure drag. This drag coefficient is not influenced by the aspect ratio. C_D is at a minimum at small C_L , increases slowly until the stall, after which it increases very rapidly. In fig. 2.17b, the points are corrected to $A = 5$ by the use of $C_{D_i} = (C_L^2)/(\pi A)$; these corrected results are plotted against the new drag coefficient C'_D for $A = 5$ given by

$$C'_D = C_D + \frac{C_L^2}{\pi} \left(\frac{1}{5} - \frac{1}{A} \right)$$

The C_{D_i} curve for an elliptical lift distribution at aspect ratio 5 is shown for comparison . Figures 2.16b and 2.17b verify, therefore, that significant departures from the elliptical distribution can be tolerated without causing appreciable corrections to the induced drag and angle of attack in the range $1 \leq A \leq 7$. However, we note that in fig. 2.16a the C_L plot for $A = 1$ has a noticeable curvature. This curvature becomes more pronounced as the aspect ratio decreases further, so the assumption that the slope a_0 is independent of angle of attack becomes more detrimental.

Chapter 3

Experimental setup

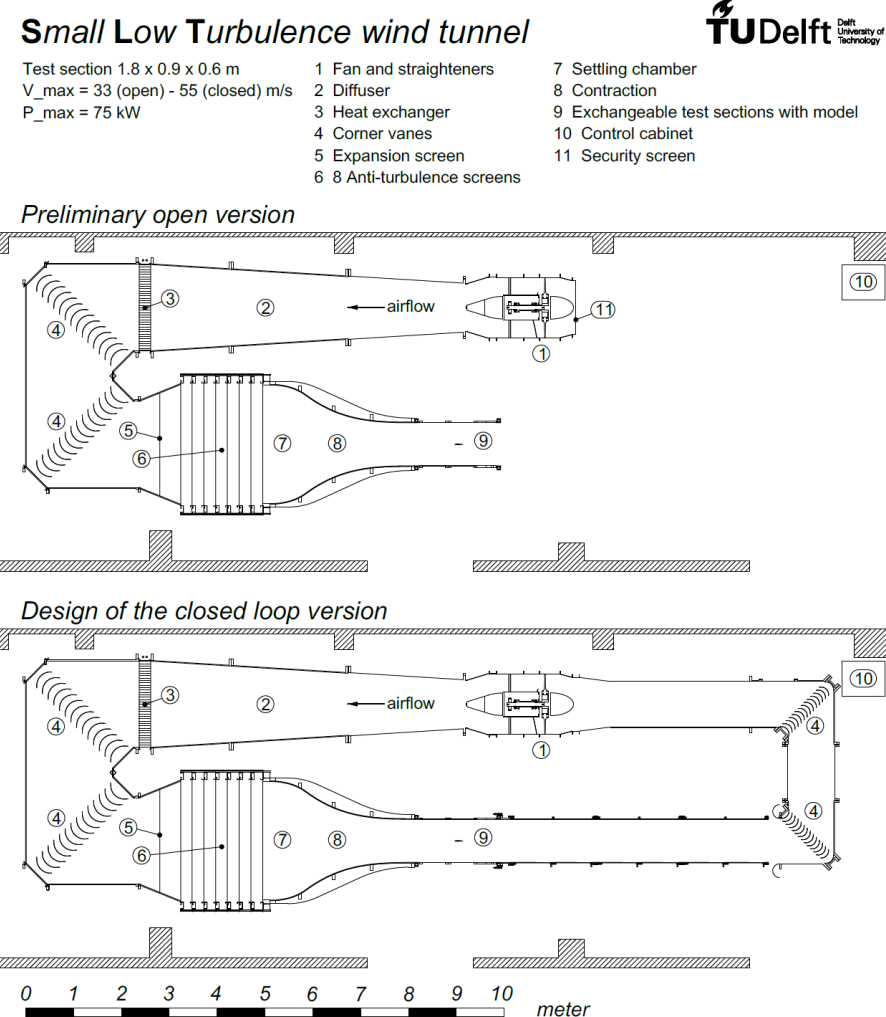


Figure 3.1: Layout of the Small Low Turbulence (SLT) wind tunnel.

3.1 Windtunnel

The windtunnel tests will be performed in the Small Low Turbulence (SLT) wind tunnel of the Faculty of Aerospace Engineering. The address of the facility is: Cornelis Drebbelweg 3, 2628CM Delft. Please refer to Appendix B for a detailed guide on how to get to the lab.

The SLT (fig. 3.1) is an atmospheric tunnel with a closed test section. The tunnel can be configured in either an open-loop or closed-loop setup. The fan is driven by a 75 kW motor, giving a maximum

test section velocity of about 33 m/s in the open-loop configuration, and 55 m/s in the closed-loop configuration. The tunnel is also equipped with a cooling system to control properties of the flow. The free-stream turbulence level (u'_{rms}/U_∞) in the test section varies from 0.06% at 20 m/s to 0.33% at 55 m/s in the closed-loop configuration. This low turbulence intensity is achieved through the use of corner vanes, which help guide the flow, and eight anti-turbulence screens mounted in the settling chamber, further reducing turbulence. Finally, the flow is accelerated through the contraction section with a high contraction ratio of 11:1. Several interchangeable test sections of 0.9 m wide, 0.6 m high and 1.8 m long are available. The usage of the tunnel is therefore efficient, since test setups can be prepared in the tunnel test section while the tunnel is fully operational.

The standard wind tunnel testing equipment consists of fluid multi-manometers, a force balance, an electronic pressure scanner system, hot wire anemometry and PIV systems. For flow visualization purposes an infra-red camera system is available. Data are recorded using an electronic data acquisition system.

3.2 Model

The model consists of a straight low aspect ratio wing that is attached to a turning table in a reflection plate. Model and turning table are attached to an external 3-component balance to measure lift, drag and pitching moment. Since both the plate and the wing model are washed by the flow the data are corrected for the contribution of the turntable.

To obtain the 2-dimensional airfoil characteristics the model is placed between end walls (fig. 3.2b). The pressure on the model surface as well those on the wake rake are measured with a NUB pressure measurement system. From the pressures on the model the normal force coefficient, C_n , is measured while the wake rake pressures deliver the drag coefficient, C_d (see section 2.2).

3.3 Data files

For the acquisition of the pressure data and the balance data separate programs are available. Their functional behaviour as well as their operation will be explained during the practical by your supervisor.

All relevant data are stored in *ASCII files* that can be processed further with a program of your own choice. Please note the considerations about the technical plots as presented in Appendix C.

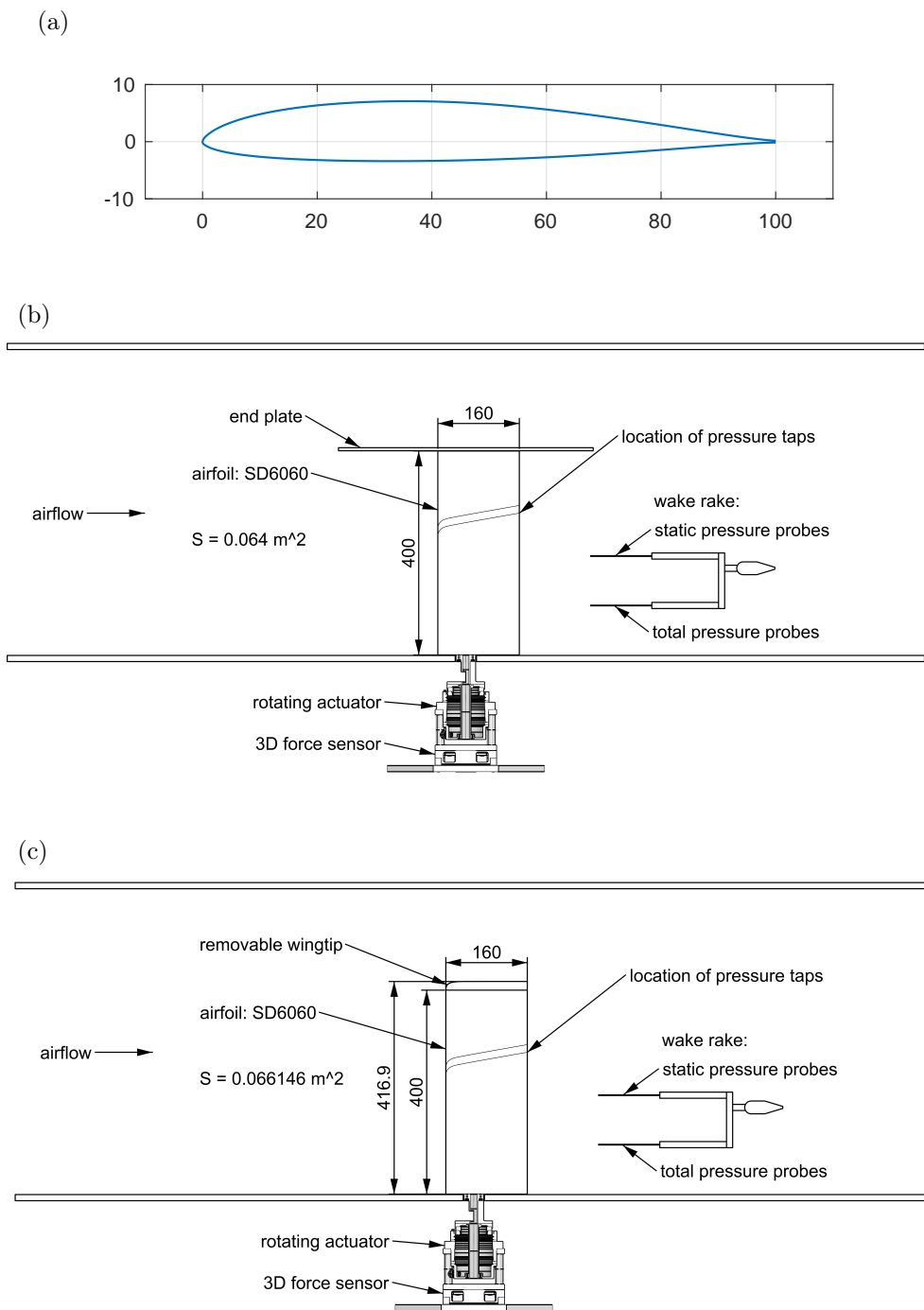


Figure 3.2: (a) SD6060 airfoil geometry; (b) 2D setup and (c) 3D setup of the straight wing model in the test section of the SLT. Length unit: mm.

Chapter 4

Numerical methods

In this chapter the applied numerical analysis method (CFD) will be discussed shortly. For detailed information the user is referred to open literature (refs. [2, 9, 11, 12]).

4.1 Numerical methods 2D

4.1.1 Aerodynamic characteristics of airfoils

Airfoils are composed of a thickness envelope over a mean camber line (Fig. 4.1).

The mean camber line lies halfway between the upper and lower surfaces of the airfoil and intersects the chord line at the leading and trailing edges.

In the past various families of airfoils were designed to show the effects of varying the geometrical variables on the important aerodynamic characteristics, such as lift, drag, and moment, as functions of the geometric angle of attack α is defined as the angle between the path and the chord line of the airfoil. The geometrical variables include the maximum camber Z_c of the mean camber line and its distance X_c behind the leading edge; the maximum thickness t_{max} and its distance X_t behind the leading edge; the radius of curvature r_0 of the surface at the leading edge; and the trailing angle between the upper and lower surfaces at the trailing edge. Theoretical studies and wind tunnel experiments have shown the effects of these variables in a way to facilitate the choice of applications. The reader is referred to Abbott and von Doenhoff (1949) for means of identifying the various families of airfoil shapes. Here we first concentrate on the geometrical features and their effect on the aerodynamic characteristics of airfoils.

To be able to design modern airfoils it is necessary to understand the basic aerodynamic characteristics. These can be studied based on rather simplified approaches. We will discuss two methods:

- Thin airfoils
- Airfoils with arbitrary thickness and camber

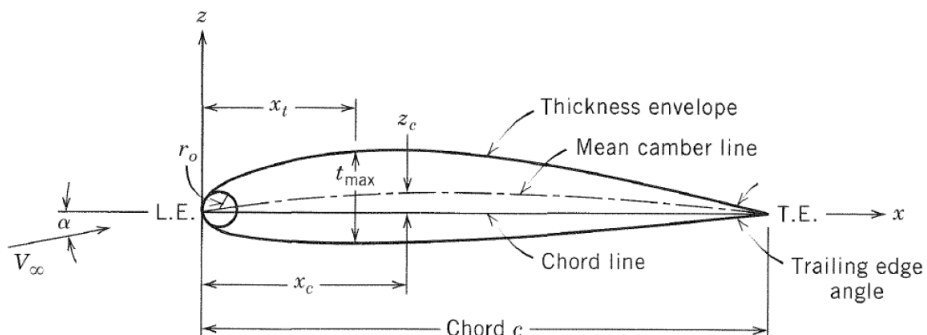


Figure 4.1: Airfoil geometrical variables.

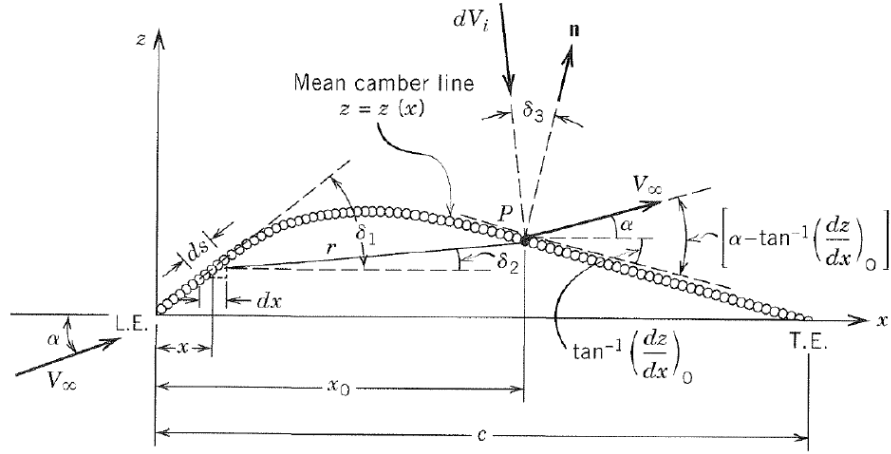


Figure 4.2: Velocity distribution for the determination of the boundary conditions of the thin wing represented by a vortex sheet.

4.1.2 Thin airfoil theory

In thin airfoil theory the airfoil thickness effects are assumed to be very small. As a result camber line of the airfoil is split in panels at which a zero normal velocity boundary condition is imposed. For the sake of completeness some additional information on this thin wing theory is presented here. Its is up to the reader whether effective use is made of this background material w.r.t. the windtunnel practical. A more comprehensive discussion can be found in open literature.

In thin-airfoil theory, the airfoil is replaced with its mean camber line. The flow pattern is built up by placing a bound vortex sheet on the camber line (Fig. 4.2) and adjusting its strength so that the camber line becomes a streamline of the flow. Points on the camber line (and therefore on the vortex sheet) lie outside the field of flow. The velocity pattern, then, is composed of a uniform stream plus the field induced by the vortex sheet.

Since the velocity difference between the upper and the lower side at the trailing edge should be zero the total strength of the sheet is fixed by the Kutta condition:

$$\gamma(TE) = 0 \quad (4.1)$$

Normal component of the velocity at every point P as indicated in Fig. 4.2:

$$dV_{in}(x_0) = -\frac{\gamma(x)ds}{2\pi r} \cos(\delta_3)$$

The negative sign is used because clockwise circulation and V_{in} along the outward unit vector \mathbf{n} normal to the upper surface are considered positive. Now use:

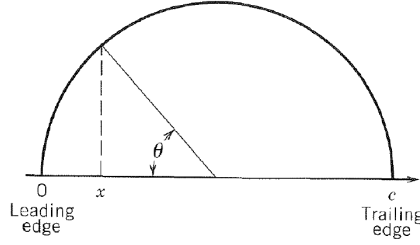
$$\begin{aligned} r &= \frac{x_0 - x}{\cos(\delta_3)} \\ ds &= \frac{dx}{\cos(\delta_3)} \end{aligned}$$

Integration from LE to TE leads to:

$$V_{in}(x_0) = -\frac{1}{2\pi} \int_0^c \frac{\gamma(x)dx}{x_0 - x} \frac{\cos(\delta_2) \cos(\delta_3)}{\cos(\delta_1)} \quad (4.2)$$

where $\delta_{1,2,3}$ are functions of x and c . The component of the free stream velocity at point P is given by:

$$V_{\infty,n}(x_0) = V_{\infty} \sin(\alpha - \tan^{-1}\left(\frac{dz}{dx}\right)_0) \quad (4.3)$$

Figure 4.3: Relation between x and c .

Here $(\frac{dz}{dx})_0$, slope of the mean chamber line $z = z(x)$ at the chordwise station x_0 , is negative at P as shown in fig. 4.2.

Again the sum of the induced and undisturbed free stream velocity component in P must be zero:

$$V_{in} + V_{\infty,n} = 0 \quad (4.4)$$

The central problem of thin-airfoil theory is to find a γ distribution that satisfies Eqs. (4.1) and (4.4). In the next section, a simplification of Eq. (4.4) is introduced that leads to the concept of the planar wing.

4.1.3 Planar (symmetrical) airfoil

In case the maximum camber is small (which is usually the case) the angles δ_1, δ_2 and δ_3 are small as well. Then eq. 4.2 becomes:

$$V_{in}(x_0) = -\frac{1}{2\pi} \int_0^c \frac{\gamma(x)dx}{x_0 - x} \quad (4.5)$$

This represents the velocity induced on the x axis by a vortex sheet lying on the x axis. Therefore, the simplification introduced above is equivalent to satisfying boundary conditions on the x axis instead of at the mean camber line. If we accept small angles of attack eq.(4.3) becomes:

$$V_{\infty,n}(x_0) = V_{\infty}(\alpha - (\frac{dz}{dx})_0)$$

And the boundary condition becomes:

$$\frac{1}{2\pi} \int_0^c \frac{\gamma(x)dx}{x_0 - x} = V_{\infty}(\alpha - (\frac{dz}{dx})_0) \quad \text{for } 0 \leq x_0 \leq c \quad (4.6)$$

The condition is applied at the x axis instead of at the mean camber line. This technique, is referred to as the planar wing approximation. The integral of Eq. (4.6) has an infinite integrand at $x = x_0$. The induced velocity is the principal value of this integral (see open literature).

4.1.4 Symmetrical airfoil properties

In case of a symmetrical airfoil the camber is zero. For convenience we transfer to a different coordinate system. In fig. 4.3 we see that:

$$x = \frac{1}{2}c(1 - \cos(\theta))$$

where c is the chord of the airfoil.

Then the conditions to satisfied are:

$$\gamma(\pi) = 0$$

$$\frac{1}{2\pi} \int_0^\pi \frac{\gamma(x) \sin(\theta) d\theta}{\cos(\theta) - \cos(x_0)} = V_{\infty}\alpha \quad \text{for } 0 \leq \theta_0 \leq \pi \quad (4.7)$$

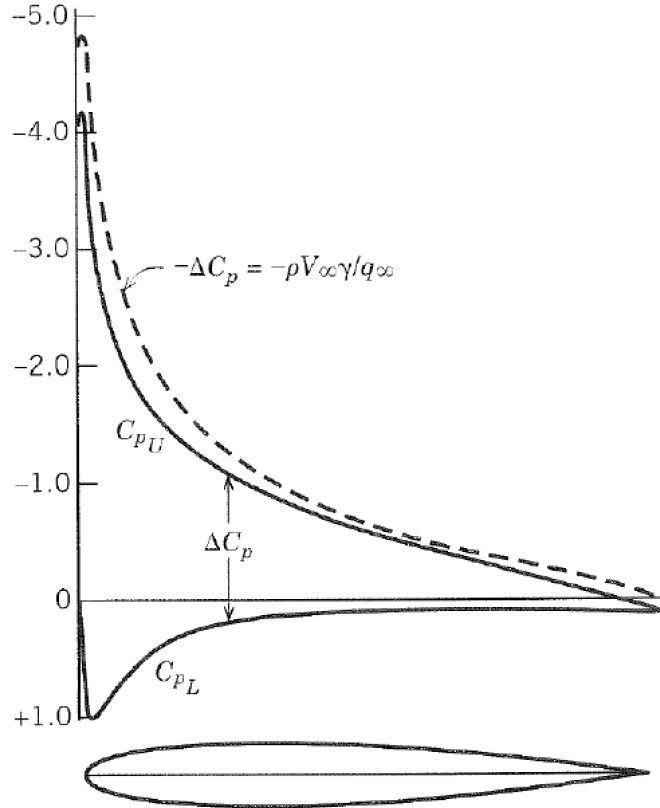


Figure 4.4: Pressure difference between upper and lower side of a NACA0012 airfoil at $\alpha = 9^\circ$.

The vorticity distribution that satisfies (4.7) is:

$$\gamma(\theta) = 2\alpha V_\infty \frac{1 + \cos(\theta)}{\sin(\theta)} \quad (4.8)$$

Using the definite integral (Prandtl):

$$\int_0^\pi \frac{\cos(n\theta)}{\cos(\theta) - \cos(\theta_0)} d\theta = \pi \frac{\sin n\theta}{\sin \theta_0} \quad (4.9)$$

and $n = 1$ we see that:

$$\int_0^\pi \frac{1 + \cos(\theta)}{\cos(\theta) - \cos(x_0)} d\theta = \pi$$

which satisfies the second of eq. (4.7). To show that 4.8 satisfies the first of eq. (4.7) evaluate the intermediate for when $\theta \rightarrow \pi$. In terms of x the vorticity distribution becomes:

$$\gamma(x) = 2\alpha V_\infty \sqrt{\frac{c-x}{x}} \quad (4.10)$$

The lift per unit area at a given position is given by:

$$\Delta p = \rho V_\infty \gamma$$

which is equal to the difference in pressure between the upper and lower side. An example of this pressure difference in the form of a pressure coefficient:

$$\Delta C_p = C_{p_l} - C_{p_u} = \frac{\rho V_\infty \gamma}{q_\infty}$$

for an NACA0012 airfoil is presented in fig. 4.4.

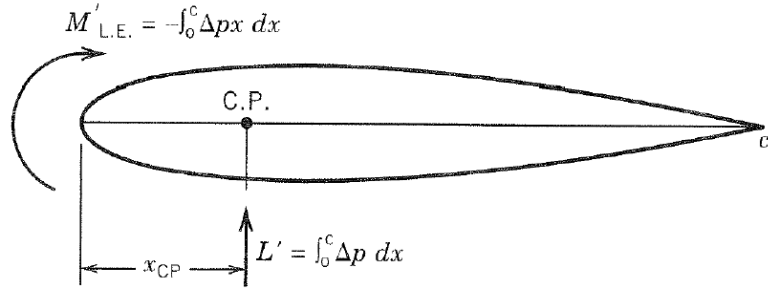


Figure 4.5: Pitching moment about the leading edge of an airfoil.

The lift per unit span l' follows from :

$$l' = \int_0^c \Delta p dx = \rho V_\infty \int_0^c \gamma dx$$

Apply the distribution of eq. (4.8) and define the local lift coefficient as

$$C_l = \frac{l'}{q_{\infty c}}$$

Then:

$$C_l = 2\pi\alpha = a_0 \alpha \quad (4.11)$$

where a_0 is the two-dimensional lift curve slope of the airfoil in case the angle of attack is given in radians.

The moment of the lift about the leading edge of the airfoil is given by:

$$M'_{LE} = - \int_0^c \Delta p dx$$

Remember that a tail down moment is defined as being positive. With the pitching moment coefficient $C_{m_{LE}} = M'_{LE}/q_{\infty c}c$ we find (see fig. 4.5):

$$C_{m_{LE}} = -\frac{\pi\alpha}{2}$$

Hence in terms of the lift coefficient:

$$C_{m_{LE}} = -\frac{1}{4}C_l \quad (4.12)$$

Apparently the centre of pressure (the point at the airfoil about which $C_m = 0$) is located at:

$$x_{cp} = \frac{c}{4}$$

at all angles of attack of the airfoil.

As a result of the assumption of a thin airfoil the pressure distribution is very peaky close to the nose which means that any effects of thickness distribution on the pressure distribution and the subsequent development of the boundary layer is neglected. This leads to a limited prediction accuracy of the airfoil lift coefficient. The analysis of a thin airfoil with camber is performed along the same line and it involves some additional (camber) angles. Its discussion is felt beyond the scope of this lab manual.

4.1.5 Inviscid/Viscous 2D panel code (XFOIL or XFLR5)

A much better approach for the calculation of 2-dimensional airfoil characteristics is obtained by positioning surface singularity on the surface instead of the camber lines such that the effect of airfoil thickness is taken into account.

The analytical method of previous sections have given remarkably accurate results for thin airfoils. However, in practice airfoils may have considerable thickness and strong interaction with other parts

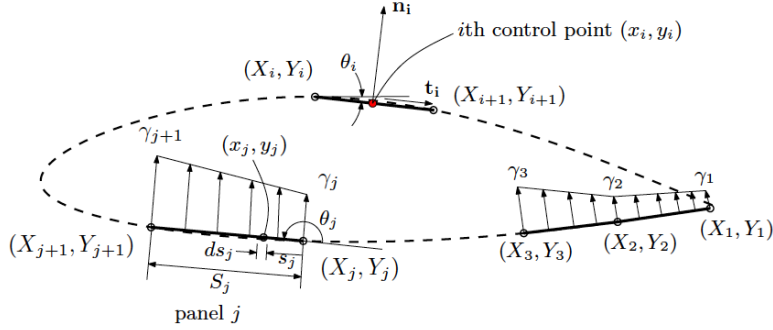


Figure 4.6: Vortex panel representation of a cambered airfoil with thickness.

of the aircraft may occur. The determination of the aerodynamic characteristics of thick, highly cambered, slotted surfaces, with single or multiple flaps and mutual interference effects among wings, fuselages, nacelles, and so forth, require, the use of numerical methods such as the *panel representation*. However the method described there applies only to non-lifting bodies. To treat lifting bodies it is necessary to introduce circulation, the strength of which is fixed by the Kutta condition.

The following method is an example on of the use of the panel method. It involves representation of the airfoil by a closed polygon of vortex panels. In case an airfoil or wing is to be analyzed the problem can be solved by means of a so-called vortex-panel distribution. For the calculation of fuselage and nacelle characteristics and their interaction the use of source and, possibly, doublet as well as vortex panels are required. The vortex-panel method is introduced here to provide a typical example of a surface singularity method. In the case presented hereafter the circulation density on each panel varies linearly from one corner to the other and is continuous the corner as indicated in fig. 4.6.

A total of m panels are positioned on the airfoil contour sequentially numbered in the clockwise direction and starting at the trailing edge. The boundary points selected on the surface of the airfoil, are the intersections of vortex panels. The boundary condition are applied ensures that the airfoil becomes a streamline. This condition is met in an approximate sense through the requirement that the normal velocity component at the mid-panel control points, V_n , becomes zero.

The velocity potential at the i^{th} control point (x_i, y_i) becomes :

$$\phi(x_i, y_i) = V_\infty(x_i \cos \alpha + y_i \sin \alpha) - \sum_{j=1}^m \int_j \frac{\gamma(s_j)}{2\pi} \tan \left(\frac{y_i - y_j}{x_i - x_j} \right) ds_j \quad (4.13)$$

where

$$\gamma(s_j) = \gamma_j + (\gamma_{j+1} - \gamma_j) \frac{s_j}{S_j} \quad (4.14)$$

Here (x_j, y_j) represent the coordinates of an arbitrary point on the j^{th} panel of length S'_j which is at a distance s_j measured from the leading edge of the panel. The integration is performed along the entire panel from (X_j, Y_j) to (X_{j+1}, Y_{j+1}) . Note that the capital letters denote the coordinates of the boundary points. The $(m+1)$ values of γ_i at the boundary points are the unknowns to be determined numerically.

The boundary condition requires that the velocity in the direction of the unit outward normal vector n_i is zero at the i^{th} control point:

$$\frac{\partial}{\partial n_i} \phi(x_i, y_i) = 0 \quad \text{for } i = 1, 2, \dots, m$$

The final result of such an analysis leads to a system equations in n unknown circulation strengths at the n panels which can be solved in a closed form.

With the circulation densities known the (tangential) velocity and the pressure at the control points can be calculated. For this purpose t_i designates the unit tangential vector on the i^{th} panel, The local dimensionless velocity is defined by:

$$V_i = \frac{\frac{\partial \phi}{\partial t_i}}{V_\infty}$$

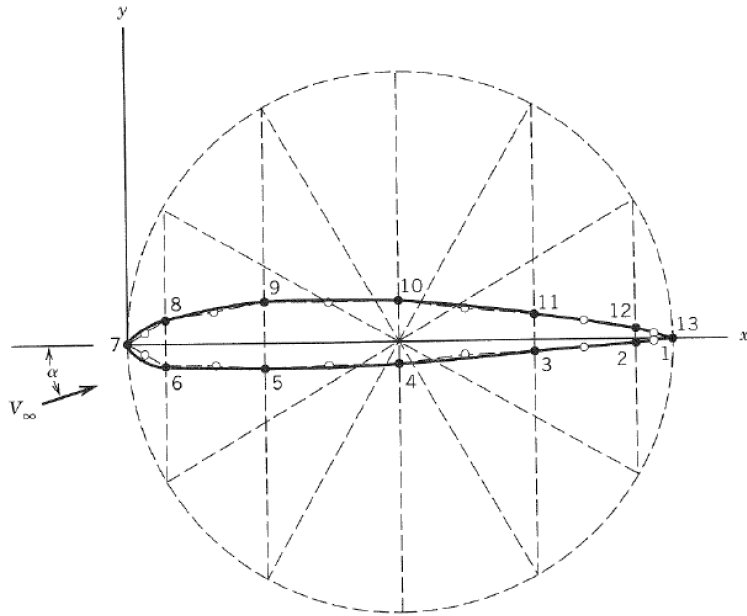


Figure 4.7: Simplified approach for the determination of a panel boundary points on an airfoil.

The pressure coefficient at the i th control point can now be calculated with:

$$C_{p_i} = 1 - V_i^2 \quad (4.15)$$

Fig. 4.7 shows a simple and yet reliable method for selecting boundary points on the airfoil. A circle centered at the mid-chord is drawn, which passes through both leading and trailing edges. When 12 panels are used in the present example, the circumference of the circle is divided into 12 arcs of equal length. Projection of the points on the circle gives 12 boundary points on the surface of the airfoil.

The trailing edge is named twice as both the first and thirteenth boundary points, as shown in fig. 4.7. A closed polygon of 12 panels is thus formed by connecting these boundary points. In this way, relatively short panels are automatically obtained in the leading- and trailing-edge regions, where changes in surface curvature are large. The results of a potential flow calculation with 12 and 50 panels is presented in fig. 4.8

It reveals that the number of 12 panels is much to low to describe the potential pressure distribution accurately. However the 50 panel variant already produces a quite acceptable result.

The total lift of the airfoil can be computed using the Kutta-Joukowski theorem in which the total circulation around the airfoil is the sum of contributions from all vortex panels. Such a computation is straightforward. The panel method outlined here is considerably more cumbersome than exact methods, such as the so-called conformal mapping technique for a single airfoil. However, the great power of the method emerges for flow calculations on multiple surfaces, such as airfoils with flaps and slots or cascades representing axial compressors or turbines and many other problems for which exact methods are not available.

The effect of viscosity can be added by performing a boundary layer calculation over the upper and the lower side of the airfoil starting in the stagnation point. Since the theoretical background of such a procedure will be treated in later lectures its discussion will be left out in this manual. However it may be important to realize that an addition of the calculated so-called boundary displacement thickness that is added to the original airfoil contour may lead to quite accurate lift and drag predictions. An example of a program that performs this type of calculations in 2D flow over airfoils is the well known XFOIL program, developed by Mark Drela from MIT (ref. [10]). In the CFD part of this practical you will be using this program for some preliminary analysis of the wing's airfoil, NACA64A2015.

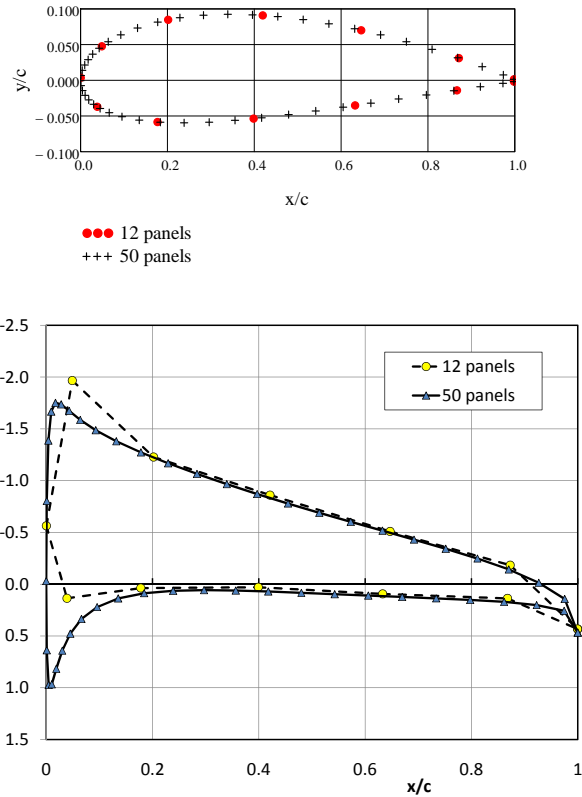


Figure 4.8: Pressure distribution over 12 and 50 panel NACA2515 airfoil based on a surface vorticity distribution over the surface.

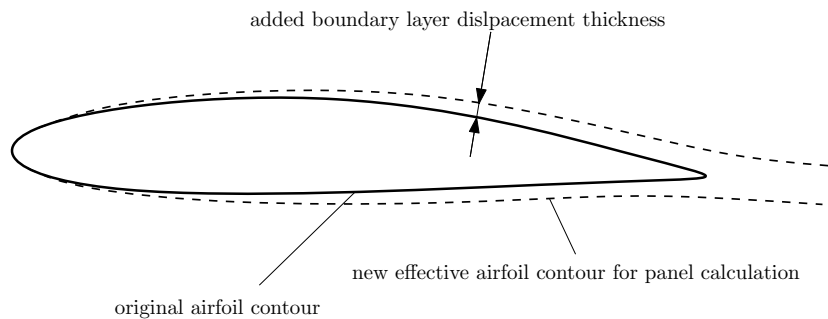


Figure 4.9: Effective airfoil contour as used in the XFOIL panel calculations. The added boundary layer displacement thickness follows from a separate solution of the so called *boundary layer equations*.

4.2 Simple Numerical methods in 3D

4.2.1 Lifting Line Theory

The lifting line theory is described in detail in ref. [1] Chapter 5. Here only the most important features and results will be summarized.

We could try using 2-D flow results for each wing section, but correct them for the influence of the trailing vortex wake and its downwash. First remember that for 2-D flow we found:

$$C_l = 2\pi\alpha$$

With

$$l = \rho V_\infty \Gamma$$

we find:

$$\Gamma = \pi c V_\infty \alpha \quad (4.16)$$

Hence, to obtain the bound vorticity strength on all spanwise sections if we need to determine the local angle of attack, α . The angle of attack used here is reduced through the effects of downwash so that the effective angle of attack becomes:

$$\alpha_{eff} = \alpha_{geo} - \frac{w_{ind}}{U_\infty}$$

Where the local induced downwash, w_{ind} , is given by the Biot-Savart Law:

$$\frac{w_{ind}(y)}{U_\infty} = -\frac{1}{4\pi U_\infty} \int_{-b/2}^{b/2} \frac{\left(\frac{d\Gamma(y')}{dy'}\right)_{wing}}{y - y'} dy' \quad (4.17)$$

Combining eq. 4.16 and 4.17 we find:

$$\alpha_{eff}(y) = \alpha_{geo}(y) - \frac{w_{ind}(y)}{U_\infty} = \alpha_{geo}(y) + \frac{1}{4\pi U_\infty} \int_{-b/2}^{b/2} \frac{\left(\frac{d\Gamma(y')}{dy'}\right)_{wing}}{y - y'} dy' = \frac{\Gamma(y)}{\pi c(y) U_\infty} \quad (4.18)$$

With this relation the local value the bound circulation distribution can be found as along as the geometrical angle of attack distribution is known.

Eq. 4.18 can be solved by assuming that the lift distribution can be expressed in a Fourier series:

$$l(y) = \frac{4}{\pi b} \sum_{n=1}^{\infty} A_n \sin n\theta$$

where $y = \frac{b}{2} \cos \theta$. Hence for the circulation we find:

$$\Gamma(y) = \frac{l(y)}{\rho U_\infty} = \frac{4}{\pi \rho U_\infty b} \sum_{n=1}^{\infty} A_n \sin n\theta$$

Substitution in eq. 4.18 then finally leads to:

$$\frac{2}{\pi^2 qbc} \sum_{n=1}^{\infty} A_n \sin n\theta = \alpha_{geo} - \frac{1}{\pi qb^2} \sum_{n=1}^{\infty} n A_n \frac{\sin n\theta}{\sin \theta}$$

The solution of this equation for all values of y is not quite so easy and generally it is determined numerically. However, an interesting and simple result appears when we restrict ourselves to special forms of the load distribution, for example the well known elliptical loading.

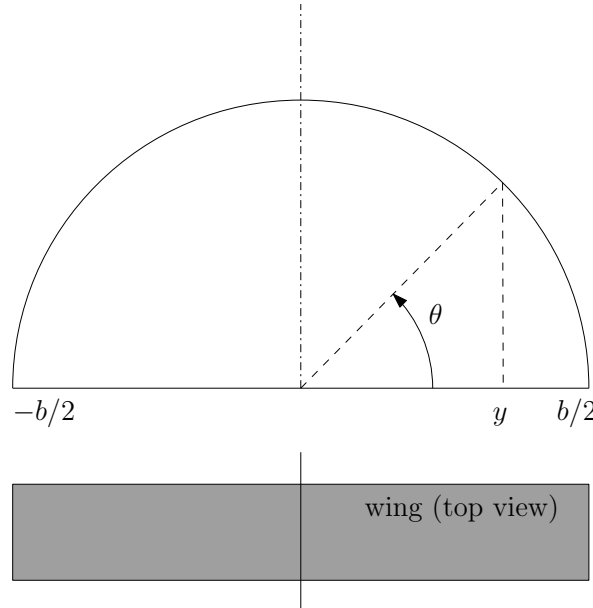
In this case we find (see ref. [1]):

$$C_L = 2\pi \left(\alpha - \frac{C_L}{\pi A} \right)$$

where A is the wing aspect ratio, $A = b^2/S$. The second term between brackets arrives from the fact that the downwash behind the elliptically loaded wing is constant. The lift coefficient thus becomes:

$$C_L = \frac{2\pi A}{A+2} \alpha = 2\pi \left(\frac{A}{A+2} \right) \alpha$$

As we can see the lift curve slope drops quickly for low values of A .

Figure 4.10: Relation between y and θ .

4.2.2 Non-linear lifting Line Theory

An extension of the classical lifting line theory is the non-linear version that makes use of the fact that in a real viscous flow the sectional lift gradient, a_0 , may deviate from the thin wing value of 2π . The computation of a real 3D wing flow using complex CFD methods is not easy can be quite time consuming. Much simpler linearized methods for example panel methods, can not give the requested results in the nonlinear areas. A simple non-linear method might be an interesting solution. The method separates acquisition of the two dimensional airfoil section aerodynamic characteristics and the computation of the three-dimensional wing characteristics. The airfoil nonlinear lift curves are acquired separately and independently on the wing computation, for example by 2D computation or by windtunnel testing, and then are used as input for the computation of wing characteristics.

It is obvious from the principle of the method that the accuracy and thus usefulness of the 3D results depend on the quality of airfoil section characteristics used as the input data and on the density and distribution of locations where the 2D airfoil characteristics are available. Moreover, the 2D airfoil characteristics close to the wing are in fact not applicable due to the strong 3D flow effects which is not accounted in the 2D airfoil analysis.

4.2.3 Vortex Lattice Code

The so-called Vortex Lattice Method (VLM) is a simplified form of the surface singularity method (often denoted as Panel Method). In this approach the surface of the wing is covered with quadrilateral panels as shown in fig. 4.11

A general description of VLM is readily available in open literature (refs. [1, 5]). The basic actions that are involved are:

1. Divide the plan form up into a lattice of quadrilateral panels, and put a horseshoe vortex on each panel
2. Place the bound vortex of the horseshoe vortex on the 1/4 chord element line of each panel.
3. Place the control point on the 3/4 chord point of each panel at the midpoint in the spanwise direction (sometimes the lateral panel centroid location is used).
4. Assume a flat wake (the usual classical method)
5. Determine the strengths of each vortex element Γ_n , required to satisfy the boundary conditions by solving a system of linear equations.

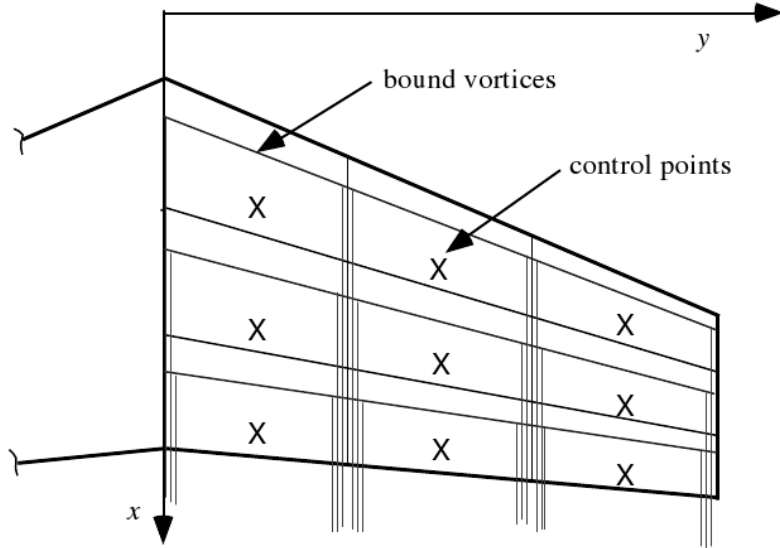


Figure 4.11: Division of the wing into quadrilateral panels.

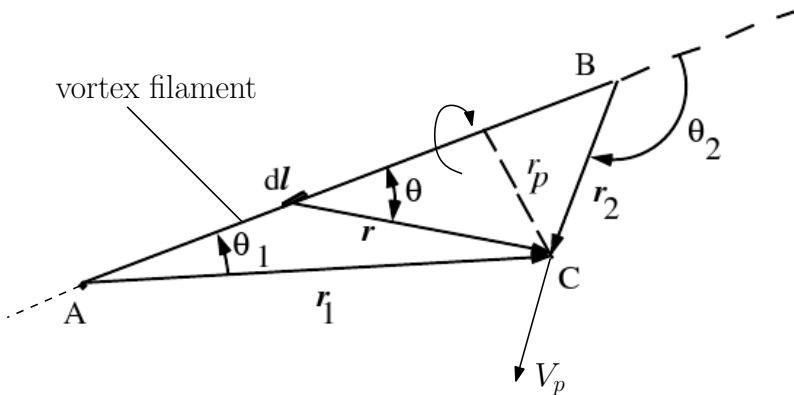


Figure 4.12: Finite vortex filament used in the determination of induced velocities.

The velocities that are induced at the location of the control point follow from the Biot-Savart law as is sketched for a finite Length vortex filament in fig. 4.12. The induced velocity of such an element is given by:

$$\mathbf{V}_p = \frac{\Gamma}{4\pi h} (\cos \theta_1 - \cos \theta_2) \mathbf{e}$$

As with the lifting line analysis the boundary condition that is applied is that of zero normal velocity at the control points:

$$\mathbf{V} \cdot \mathbf{n} = 0 \quad (4.19)$$

The velocity vector V is determined completely by the geometrical layout of the wing and the effective velocity vector at every control point, m :

$$V_m = (V_\infty \cos \alpha \cos \beta + u_{m_i}) \mathbf{i} + (-V_\infty \sin \beta + v_{m_i}) \mathbf{j} + (V_\infty \sin \alpha \cos \beta + w_{m_i}) \mathbf{k}$$

where the terms with V_∞ is the local contribution of the undisturbed incoming flow speed (the angles α and β are the angle of attack and the angle of yaw, respectively). With the given lattices (panels) and the boundary conditions of eq. 4.19 a closed system of equations is found in which the vortex strength of the panels, Γ_i . The resulting system of equations has the following general form¹:

$$\sum_{n=1}^{2N} C_{m,n} \left(\frac{\Gamma_n}{V_\infty} \right) = \left(\frac{df_c}{dx} - \alpha \right) \quad m = 1, 2, 3, \dots, 2N$$

where $C_{m,n}$ is the influence coefficient of vortex element n on panel m , N is the number of panels per wing side and f_c denotes the function that describes the position of the camber line in space.

¹A more elaborate discussion can be found in many text books. This is felt beyond the scope of this manual.

Setting up such a VLM system is not difficult but it requires quite some programming because:

- In general an automatic layout of panels for arbitrary geometry is required. As an example, when considering multiple lifting surfaces, the horseshoe vortices on each surface must “line up”. The downstream leg of a horseshoe vortex cannot pass through the control point of another panel as this will lead to singular behaviour of the model (the program can not cope with division by zero or calculation with infinite induced velocities close to the core of a vortex filament)
- The conversion of the local circulation strengths, Γ_i into aerodynamic wing characteristics like C_L , C_D and C_m and the lift distribution is quite laborious for arbitrary configurations.

For this reason during the practical use will be made of existing software that can be found on the Internet (AVL and XFLR5) and which is known to provide quite accurate results (of course within the range of applicability).

Chapter 5

Post-processing and reporting

5.1 Introduction

To arrive at a clear and meaningful discussion of all aerodynamics aspects encountered during this lab it is mandatory to write a report. This report has some minimum requirements which are explained underneath. Make sure that you perform the given tasks and address the presented problems both as a group and as an individual. In case you need additional information please check the manual that can be found on the Brightspace pages. Your supervisor that guides you through the practical is the first point of contact for any matter related to this windtunnel test.

With the experimental and the numerical data available the post-processing step becomes an extremely important step in the reporting process. During this phase the true “quality” of the data become imminent and important conclusions may be drawn about the validity of the methods used (both experimental and numerical). The post-processing not only requires clear and descriptive text where the results are discussed but also graphical elements (graphs, sketches, etc.) to support the findings. In this respect it is advised to put quite some effort in the quality and clarity of the plots. Typical examples can be found in open literature (text books and scientific articles). To provide some advise in this matter typical requirements for graphs are discussed in Appendix C. Do not underestimate this part of the post-processing step in the final grading of your work.

5.2 Work-load reporting

A clear report should be written as a deliverable for this practical. The report should be delivered as group work (1 report per group). In the appendix of the report there should be a list indicating the individual contribution of each member. In case some sections are work of two or more members this should be indicated in the list. It is up to the team to decide how to split the work.

5.3 Deadlines

The following deadlines apply strictly:

- **Report delivery:** The final, completed report should be delivered within **3 weeks** from the day of the performed practical

5.4 Tasks

Please perform the following tasks while working out the windtunnel test and the associated CFD analyses.

1. Gather all the measured and calculated data in a clear overview and discuss the main results **within the group**. Make sure that everyone agrees with the contents and the quality of the data and distribute the data among group members. **Additional CFD calculations that are performed after the lab should also be distributed.**
2. Set up a "task distribution list" for all group members. Make sure that tasks are fairly distributed among the team members. This is the task of your group alone. Your supervisor is not responsible for task allocation.
3. Write a report (1 per group) in which **the goal, setup, and results of the practical are presented. Draw relevant conclusions in a separate chapter or section**. The typical contents of the report is presented in section 5.5.
4. It is **compulsory to include a list of task allocation in the appendix of your report**. This should be as detailed as possible. It should be clear from the list which team member contributed to which task. This will help your supervisor to identify if the work load has been shared in a fair way and give the appropriate grade.
5. **Deliver the report to the email address of your supervisor within 3 weeks** after the test date. After it has been accepted (approval by supervisor) your grades will be communicated to you by your supervisor. If you need further discussion you should arrange a meeting with your supervisor.
6. In case you have objections regarding the grade then an oral exam can be arranged. Keep in mind that depending on your performance at the oral exam your grade can go both up and down.

5.5 Typical contents of the lab report and rubrics

Please refer to the instructions for the lab report (a separate document on Brightspace).

Bibliography

- [1] J.D. Anderson, "Fundamentals of Aerodynamics", Mc Graw Hill, 4th edition, 2005
- [2] RT0 Applied Vehicle Technology Panel, "A Feasibility Study of Collaborative Multi-facility Windtunnel Testing for CFD Validation", RT0 TECHNICAL REPORT 27, 1999
- [3] Abbott and von Doenhoff, "Theory of Wing Sections: Including a Summary of Airfoil Data", New York, Dover publications Inc., 1959
- [4] Internet page: http://www.ae.illinois.edu/m-selig/ads/coord_database.html
- [5] J.J. Bertin, "Aerodynamics for Engineers", Fourth edition, Prentice Hall publication, 2001
- [6] H. Ashley and M. Landahl, "Aerodynamics of Wings and Bodies", Addison-Wesley, Reading, Mass. 1965
- [7] L.L.M Veldhuis and S. Nebiolo, "A propeller integration study comparing experimental data with numerical flow solutions based on the Navier-Stokes equations", ICAS-2000-2.6.4, ICAS conference, Harrogate, United Kingdom, 2000
- [8] Veldhuis, L.L.M., D.W.E. Rentema; Experimental Analysis of the Vortex Wake Structure behind a Propeller-Wing Configuration. In: AGARD FDP Symposium on "The characterisation and modification of Wakes from lifting vehicles in fluid", Trondheim, Norway, 20-23 May 1996. Published in AGARD CP-584. 1996, p. 15-17.
- [9] J. Katz, A. Plotkin, Low-Speed Aerodynamics 2nd Edition, Cambridge Aerospace Series (No. 13), ISBN: 9780521665520, March 2001
- [10] M. Drela, "XFOIL: An Analysis and Design System for Low Reynolds Number Airfoils," Conference Proceedings on Low Reynolds Number Aerodynamics, Notre Dame, Indiana, 5-7 June 1989.
- [11] J. Moran, An Introduction to Theoretical and Computational Aerodynamics , 1st edition, New York, NY: John Wiley and Sons, 2003. ISBN: 0486428796.
- [12] I. Kroo, Applied Aerodynamics: A Digital Textbook, Version 5.0, January 2007 Desktop Aeronautics, Inc., <http://www.desktop.aero/appliedaero/preface/welcome.html>

Appendix A Overview of activities during Windtunnel test AE2130-II

Experiments (on location)

- Perform windtunnel tests on the straight wing model in
 - 2D flow. In this case the wing tip is removed and pressures are measured over the model surface and in the wake (program *measE*)
 - 3D flow. The wing tip is now installed and force measurements are performed using the external balance system (program *w3d*)
- Copy the obtained data to a local drive to extract the pressure and polar data for later comparison.

Numerical Analysis (on location and at home)

- Perform calculations to predict the characteristics in:
 - 2D flow. In this case the program XFOIL is used. Both inviscid and viscous calculations are performed to determine the effects of viscosity in the real flow.
 - 3D flow. Different programs will be used to determine: the lift, drag and pitching moment coefficients, the lift distribution. The following programs will be made available (through Internet / Brightspace):
 - * *AVL*. Athena Vortex Lattice Method (VLM) code.
 - * *XFLR5*. An open source program that is capable of performing a LLT, VLM or PANEL analysis of the wing.

A short description on how to use these programs is provided in separate documents on Brightspace.

Groups

The work is performed in groups of maximum 10 students. The students are divided into subgroups of two with specific sub-tasks regarding the experiment (see Table 1)

Table 1: Overview of lab activities.

General introduction	<ul style="list-style-type: none"> • Short theory introduction • Overview of the wind tunnel equipment • Allocation of the sub-group tasks
Part 1: 2D wing	<ul style="list-style-type: none"> • Session 1: 8:30-9:00 • Session 2: 11:45-12:15 • Session 3: 15:00-15:30 <ul style="list-style-type: none"> • Initialisation of the related software • Acquisition of wall and wake pressures for the selected aoa • Visualisations using the thermal images and tuft • Conversion of the 2D setup into the 3D setup
Part 2: 3D wing	<ul style="list-style-type: none"> • Session 1: 10:00-11:00 • Session 2: 13:15-14:15 • Session 3: 16:30-17:30 <ul style="list-style-type: none"> • Initialisation of the related software • Zero-runs • Measurement of aerodynamic loads using balance • Visualisations using the thermal images and tuft • Conversion of the 3D setup into the 2D setup (for the next group)
Wrap up	<ul style="list-style-type: none"> • Session 1: 11:00-11:30 • Session 2: 14:15-14:45 • Session 3: 17:30-18:00 <ul style="list-style-type: none"> • Recap • Reporting details and deadlines • Questions

Appendix B Location

The windtunnel tests will be performed in the Small Low Turbulence wind tunnel (SLT) of the Faculty of Aerospace Engineering (figure 1). The address of the facility is: Cornelis Drebbelweg 3, 2628CM Delft. The wind tunnel is located on the second floor. Once you enter the door (figure 2) just follow the signs to the wind tunnel.

Participants are requested to be present 10 minutes before the start time of their session. Delay of more than 15 minutes from the starting time will result to exclusion from the test and a fail grade.

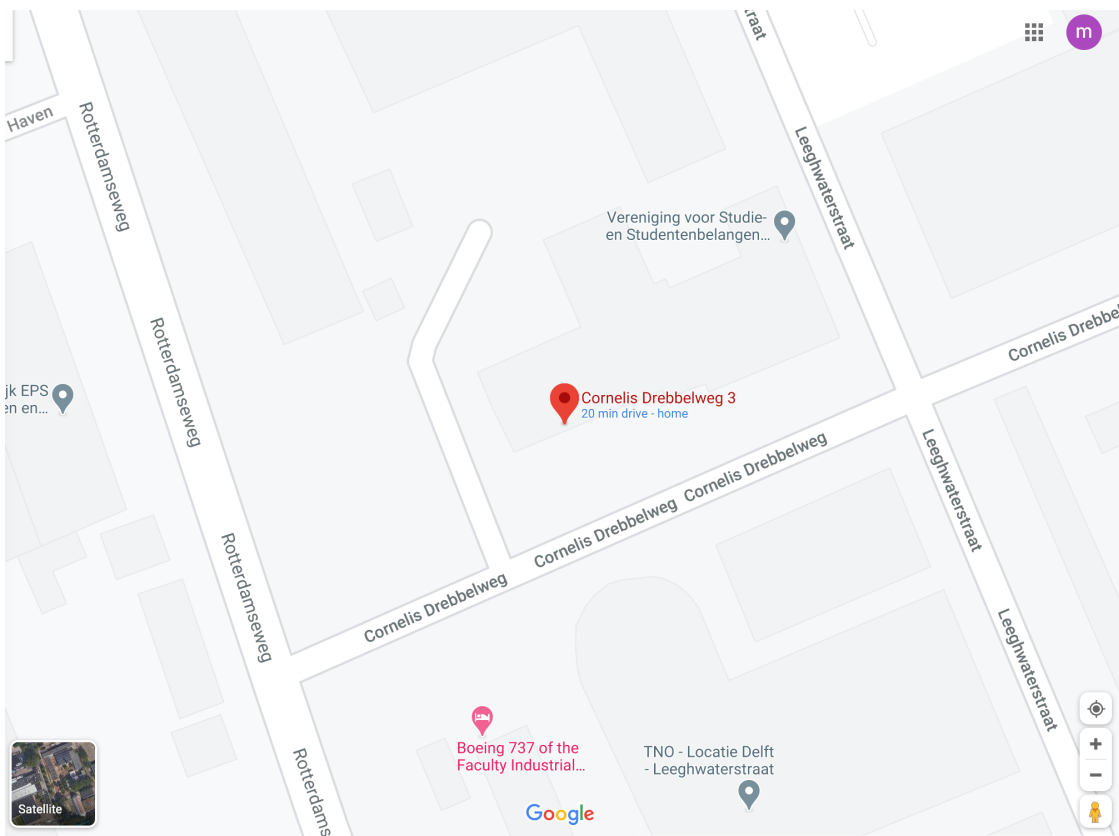


Figure 1: Location of the Low Speed Laboratory.



Figure 2: Location of the Low Speed Laboratory.

Appendix C About graphs, “the good, the bad and the ugly”¹

To convey your message to the reader it is extremely important to deliver clear and high quality graphs. Underneath you will find some examples of good (acceptable) as well as bad (unacceptable) graphs. In this case the lift coefficient of a particular wing is plotted versus the angle of attack (in degrees). The graphs contain both experimental and numerical results (VLM code). In the caption (which are put always underneath the graph and should be numbered) remarks are made about the particular aspects. Read them carefully!

¹“The Good, the Bad and the Ugly” is a classic western produced in 1966 by the famous Italian director Sergio Leone.

Good graphs

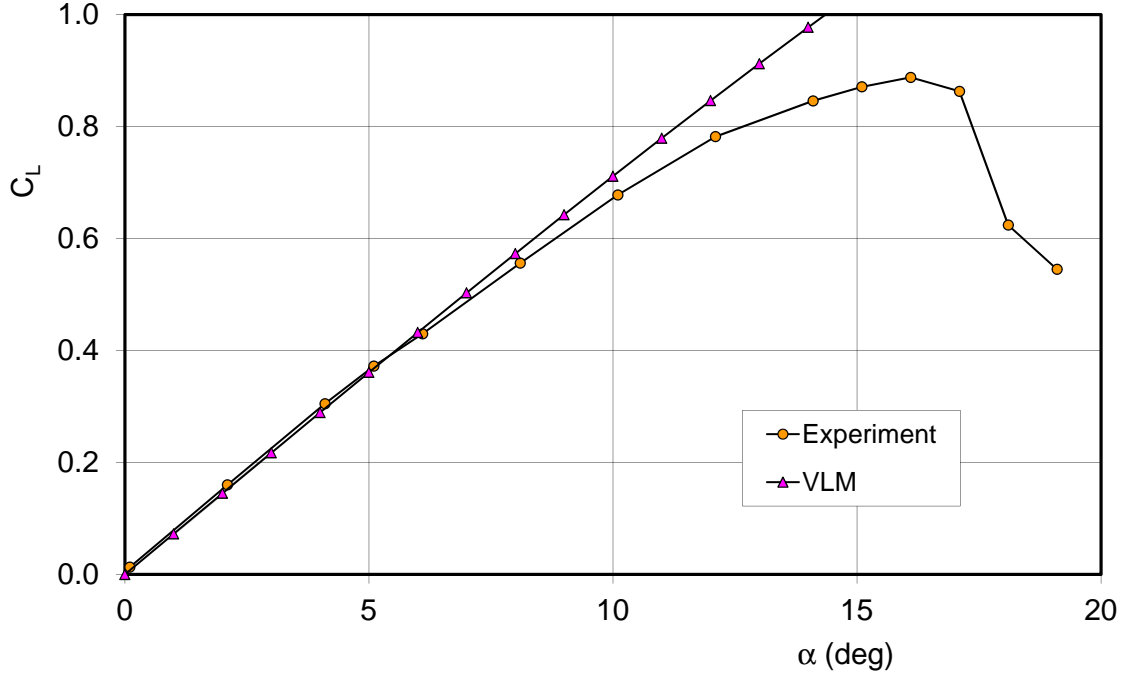


Figure 3: Lift coefficient of the LS4 model versus the angle of attack at $Re_c = 1.0 \times 10^5$. Comparison of the experimental balance data and numerical analysis.

N.B. This is a nice graph. It contains all the relevant information including a descriptive text (the caption). Since the lift coefficient changes with the Reynolds number its value is mentioned in the caption (this could also have been done in the graph itself). Furthermore we see that:

- The figure is numbered
- A legend is present
- Different colors and different symbols have been used for the two curves. Both in color and in black and white prints the two curve are clearly recognizable.
- The axis labels are correctly formatted. This includes the subscript for the lift coefficient (C_L instead of CL and α instead of alpha; the latter is wrong since it is very unlikely that “alpha” will be taken up in the list of symbols in the beginning of the report).
- The line thickness is OK. Even if the figure is scaled down the curves are discernible
- The scaling of the axes is OK w.r.t. to their range and number of digits.

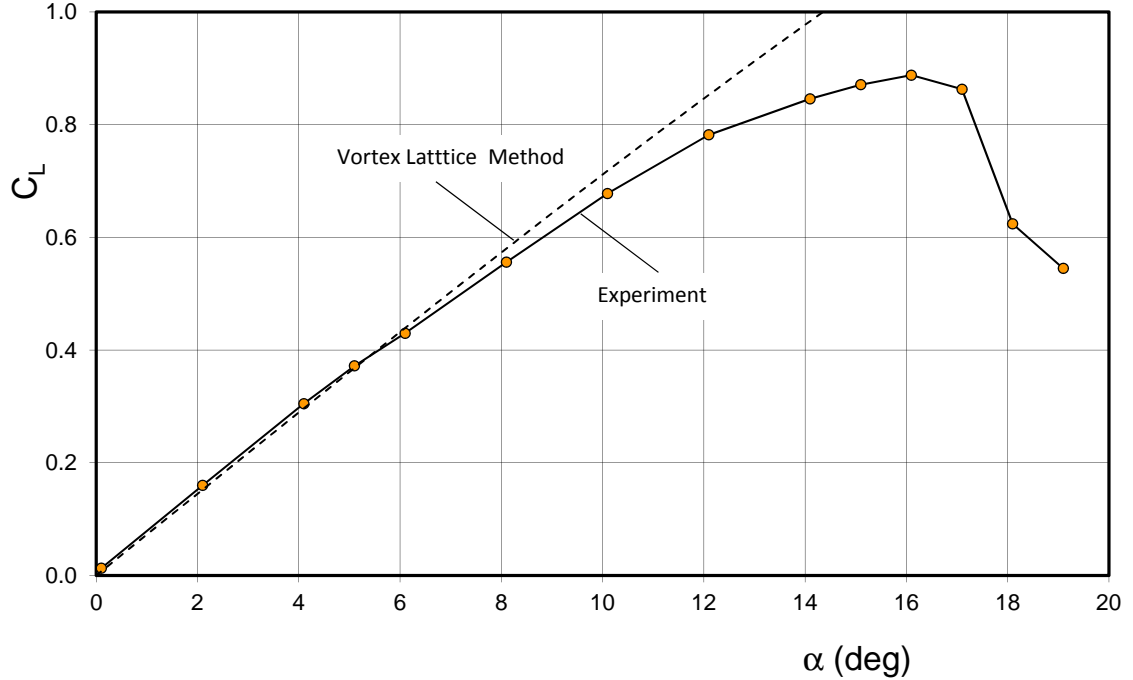


Figure 4: Lift coefficient of the LS4 model versus the angle of attack at $Re_c = 1.0 \times 10^5$.

N.B. This is also an acceptable graph.

- Instead of a separate legend box the two curves are indicated with a descriptive text
- The curve for the numerical results is dashed and contains no symbols. This indicate that the value at which C_L is determined with the VLM is not important. The VLM result, in this case, always leads to a linear behaviour.

Bad graphs

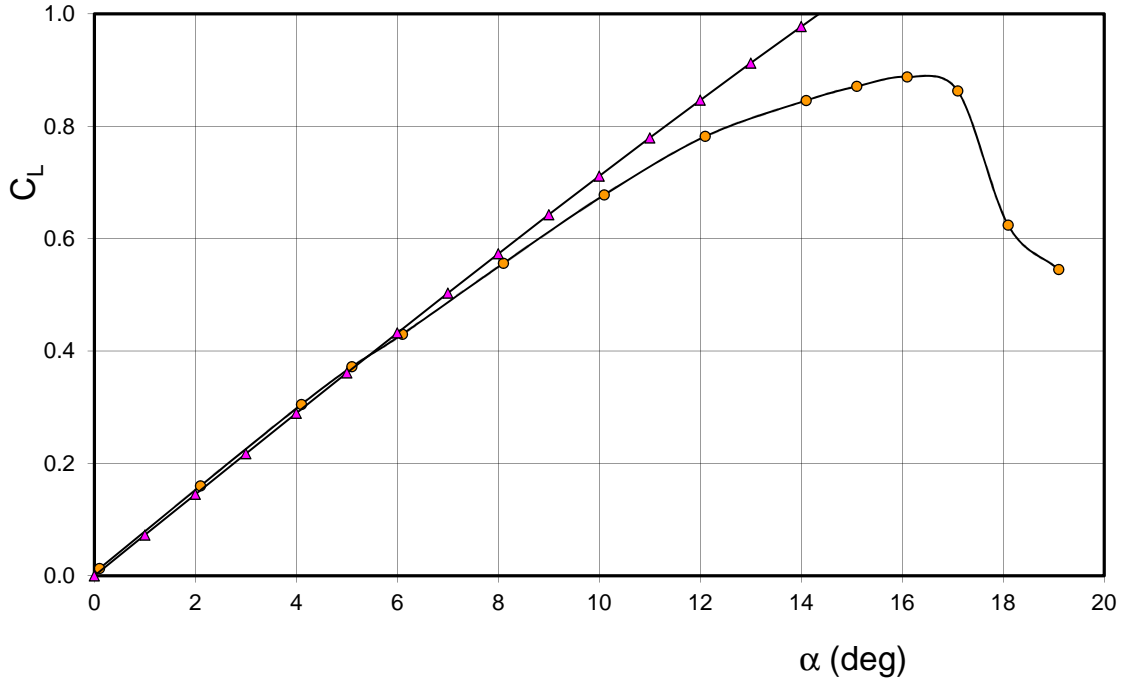


Figure 5: Lift coefficient of the model.

N.B. This is unacceptable graph! This is why:

- First of all the caption: It does not tell us which model is meant (the model?). Furthermore the Reynolds number is not mentioned. The text is simply too short to get the full meaning of the plot.
- There is no legend available
- The curve through the experimental data points is smoothed. This is not allowed since we only know the value at a limited number of α . The fact that a smoothed line is used here suggest that you know where intermediate data points are located. For the lift coefficient of a wing this may be quite predictable but in general this is quite tricky. Hence, connect the data point with straight line elements!
- Last but not least note that the font size for the axis labels etc. is quite small. In case this figure is scaled down (for example in a two-column format) the labels may become unreadable.

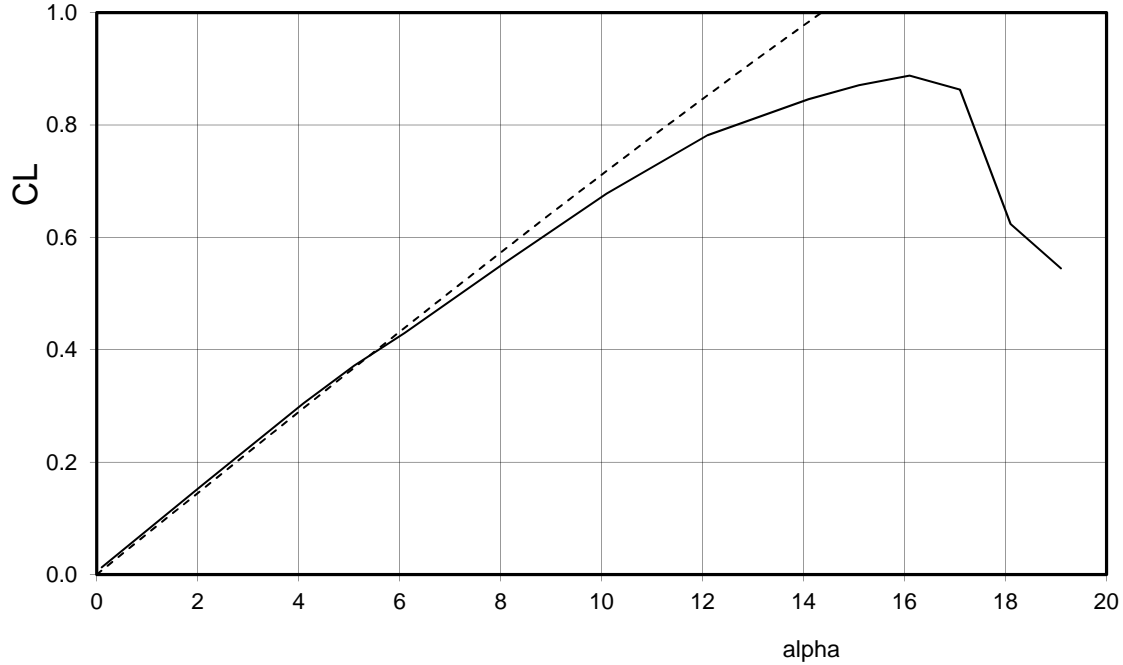


Figure 6: Lift coefficient of the model.

N.B. This is unacceptable graph! Additional to the remarks given for the previous figure:

- The curve for the experimental data does not show the data points. Hence, the reader can hardly recognize the which angles of attack where measured.
- The axis labels are not according to the required standard. The vertical axis should read C_L instead of CL while the horizontal axis should read α (deg) instead of alpha.

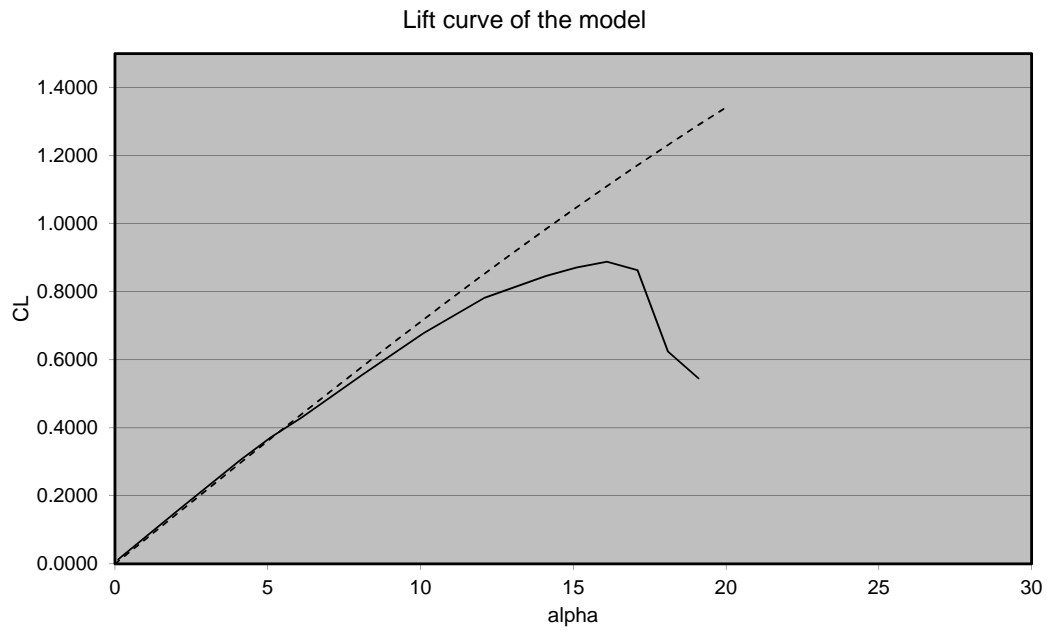


Figure 7:

N.B. This is unacceptable graph! Additional to the remarks given for the previous figures:

- *There is no caption!*
- To much white space around the plot
- The title above the graph is superfluous. Remove it.
- The axis scaling (range) is inappropriate
- The number of digits for the vertical axis is to high (use 1.4 instead of 1.4000)
- The gray background is default in Excel. It has no additional meaning and suggests that you have produced the graph quickly without considering its contents.
- In case horizontal grid lines are used also use vertical grid lines

Ugly graphs

Underneath some “ugly” graphs are presented without further comments. It is up to the reader to determine why these are unacceptable for incorporation in a scientific report.

